

We are IntechOpen, the world's leading publisher of Open Access books Built by scientists, for scientists

6,900

Open access books available

185,000

International authors and editors

200M

Downloads

Our authors are among the

154

Countries delivered to

TOP 1%

most cited scientists

12.2%

Contributors from top 500 universities



WEB OF SCIENCE™

Selection of our books indexed in the Book Citation Index
in Web of Science™ Core Collection (BKCI)

Interested in publishing with us?
Contact book.department@intechopen.com

Numbers displayed above are based on latest data collected.
For more information visit www.intechopen.com



Basics of High-Speed Electrical Machines

Flyur R. Ismagilov, Viacheslav Ye. Vavilov and
Valentina V. Ayguzina

Additional information is available at the end of the chapter

<http://dx.doi.org/10.5772/intechopen.78851>

Abstract

The high-speed electrical machines are widely used in different industries, such as machine tools, aerospace engineering, autonomous power engineering, etc. This chapter is devoted to the basics of high-speed electrical machines with high-coercitivity permanent magnets. It is considered in the application areas of high-speed electrical machines and their classifications. In addition, design problems of high-speed electrical machines are shown. To estimate the efficiency, loss calculations are performed. The obtained results can be used in the design of high-speed electrical machines with high-coercitivity permanent magnets and in their future development.

Keywords: high-speed electrical machine, high-coercitivity permanent magnets, amorphous magnetic material, eddy-current losses, windage losses

1. Introduction

The main task of electrical machine (EM) design is to provide maximum power with a minimum energy loss and volume of active and constructive elements. Reduction of the material consumption and the production technology improvement can significantly reduce the cost of electrical machines, and subsequently, the cost of the systems, where they are used (e.g., aircrafts and machine tools), or resources obtained with their help (e.g., electricity and oil). In addition, the development of new industries and the implementation of macro- and microresearch projects lead to an emergence of new tasks to reduce mass-and-size parameters and to increase the efficiency of electrical machines.

The directions that allow the solution of these problems can be determined from the analysis of the mathematical formula proposed by Engelbert Arnold in 1896 [1]:

$$P = \frac{\pi^2}{60 \cdot 10^{10} k_e} \alpha_\delta D^2 l_a B_\delta A n k_{m.f} k_w,$$

where P is EM power, A is a linear current load, D is a rotor diameter, l_a is a length of the EM, B_δ is a magnetic flux density in the air gap, n is a rotational speed, $k_{m.f}$ is a coefficient of the magnetic field shape in the air gap, α_δ is a pole pitch coefficient, and k_w is a winding coefficient.

From Arnold's equation, it can be seen that at the invariable volume of the EM elements, its power can be increased in three ways or their combinations: to increase linear current load, to increase magnetic flux density in an air gap, and to increase rotational speed of EM rotor.

All these three ways have found the niche in different industries. One of the directions is the high-speed and ultra-high-speed EMs, which are widely used in machine tools, aerospace engineering, autonomous power engineering, etc. In this chapter, high-speed and ultra-high-speed EMs are frequency-controlled EMs with high-coercitivity permanent magnets (HCPM). Section 2 presets the classification of high-speed EMs. The main application areas are presented in Section 3. Section 4 is devoted to calculation of losses and efficiency of the high-speed EMs.

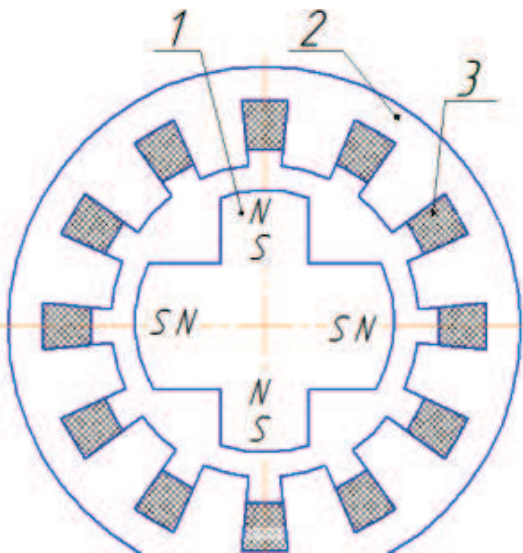
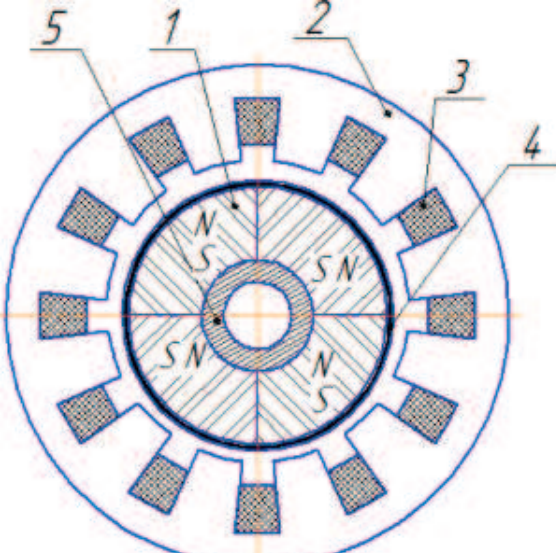
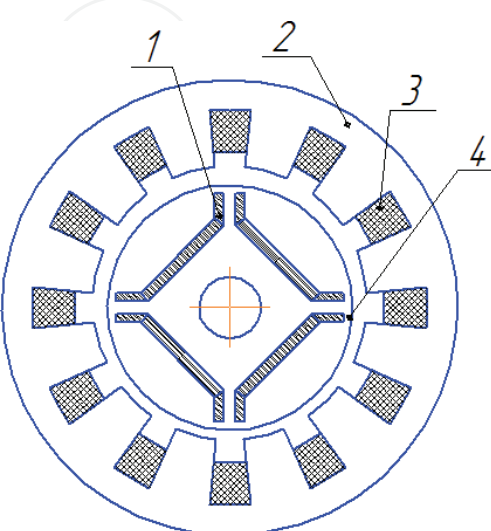
2. Classification of high-speed EMs

To develop and generalize the high-speed EM theory, their classification should be considered. In general, high-speed EMs can be classified according to the operation principle, design features, frequency or output voltage, the stator type (slotted or slotless), etc. **Table 1** shows the basic designs of high-speed EMs. The slotless stator designs are not given in **Table 1**. However, the design nos. 1–6 and 8–12 can be made with a slotless stator. The hysteresis motor designs are not presented in **Table 1**, although they are also high speed and are used in gyroscopes.

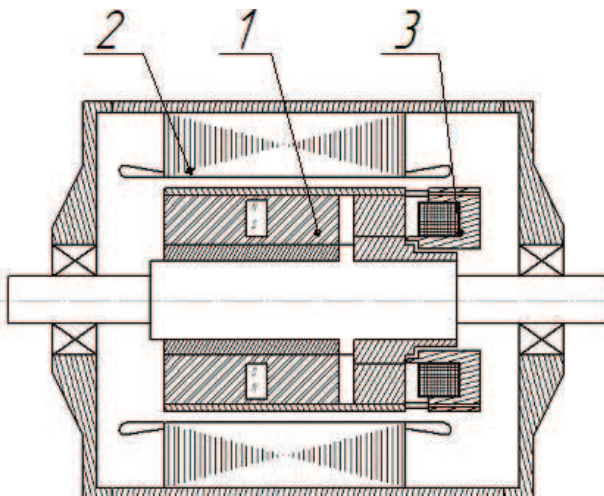
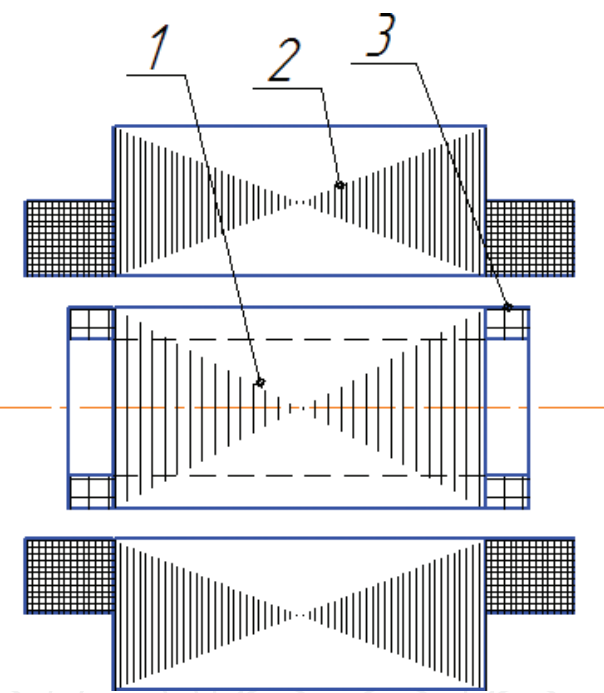
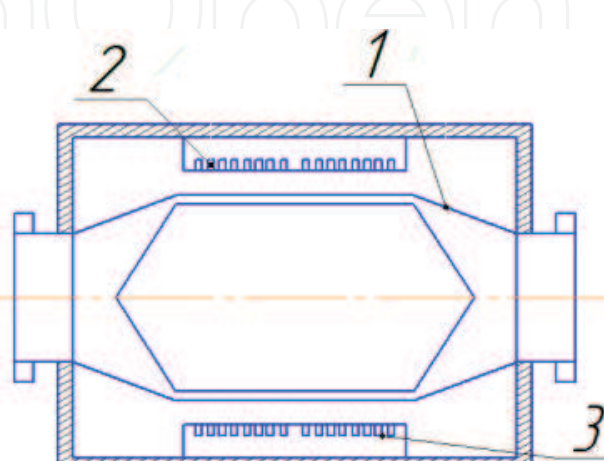
High-speed EM with electromagnetic excitation and designs nos. 5, 8, 9, 10, 11 are inferior to the high-speed EM with HCPM for reliability, specific parameters, and efficiency. However, they have some development prospects; for example, the design possibility of high-speed EM with rotating rectifiers and a rotational speed of 50,000 rpm is presented in [1, 2].

Axial EMs with HCPM can be promising for power supply systems for rocket and space equipment due to their small axial dimensions. The design and prospect review of axial EMs are presented in [3, 4]. At the same time, axial EMs have been created with rotational speed of 30,000–48,000 rpm.

In addition, the use of HCPM made of NdFeB and SmCo alloys for high-speed damping elements is promising to develop the space systems due to improving their energy characteristics [5]. To develop the alternative energy, the ship and transport systems (railway trains), including the cargo location tracking, the use of single-coordinate and multicoordinate vibrational EMs with HCPM is of interest [6, 7]. To develop the ship power supply systems, energy conversion systems of detonation engines and automotive systems, the use of high-speed linear EM with HCPM as the main generators of the power supply system is topical.

EM type	Design
1. High-speed EM with a star-type rotor: 1 is a star-type rotor, 2 is a stator magnetic core, and 3 is a stator winding	
2. High-speed EM with an assembled star-type rotor: 1 is a cylindrical HCPM, 2 is a stator magnetic core, 3 is a stator winding, 4 is a rotor sleeve, and 5 is a rotor back	
3. High-speed EM with interior permanent magnets: 1 is the HCPM, 2 is a stator magnetic core, 3 is a stator winding, and 4 is a rotor back	

EM type	Design
4. High-speed EM with combined rotor magnetic systems (including the Halbach magnetic system): 1 is the combined rotor magnetic system, 2 is the stator magnetic core, and 3 is a stator winding	
5. High-speed synchronous EM with rotating rectifiers: 1 is a rotor, 2 is a stator, 3 is a block of rotating rectifiers, and 4 is an excitation system	
6. Axial EM with HCPM: 1 is the HCPM, 2 is a stator magnetic core, and 3 is a stator winding	

EM type	Design
7. High-speed synchronous EM with combined excitation: 1 is a rotor, 2 is a stator magnetic core, and 3 is an additional excitation system	
8. High-speed asynchronous motors with squirrel-cage rotor: 1 is a rotor, 2 is a stator magnetic core, and 3 is rotor bars	
9. High-speed liquid-metal asynchronous motor: 1 is a annular channel, 2 is a ring winding, and 3 is a magnetic core	

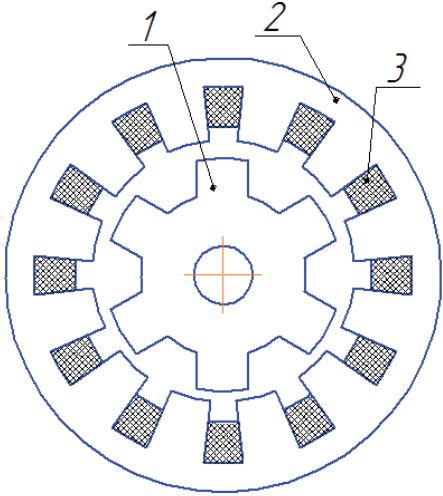
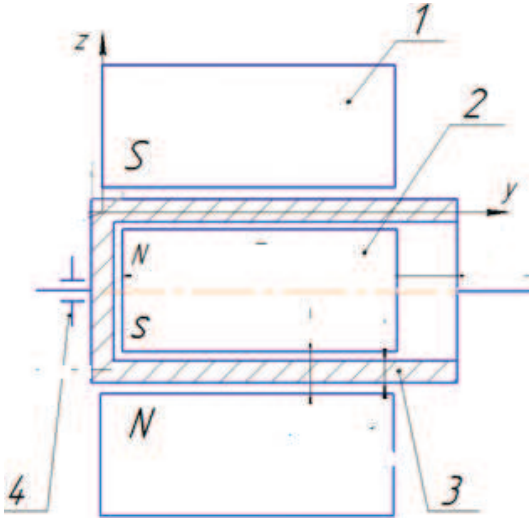
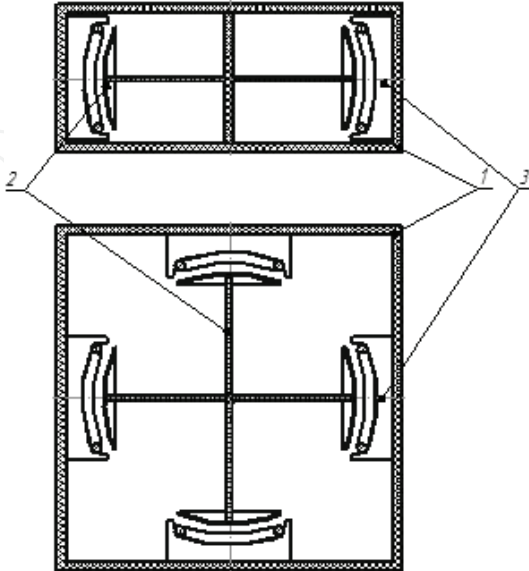
EM type	Design
10. High-speed induction EM: 1 is a rotor, 2 is a stator magnetic core, and 3 is a stator winding	
11. High-speed damping elements with HCPM: 1 is an external HCPM, 2 is an internal HCPM, 3 is a hollow rotor, and 4 is a bearing	
12. High-frequency oscillating EM with HCPM: 1 is a casing, 2 is a moving part, and 3 is a winding	

Table 1. Basic designs of high-speed EMs.

The presented classification shows that areas and prospects for the use of high-speed EM with HCPM are quite broad. The improvement of this EM type leads to an expansion of its application areas. Therefore, it seems expedient to consider in more detail the application areas of high-speed EM and to reveal their development prospects.

3. Application areas of high-speed electrical machines and a review of known works

To use the high-speed EMs, it is necessary to have a high-speed drive (for generator mode) or a high rotational speed (for motor mode). Therefore, the main application areas of high-speed EMs are high-speed machine tool, aviation and space power engineering, as well as autonomous power engineering. The initial application of high-speed EMs is associated with the development of rocket and space technology. High-speed induction and hysteresis motors with a rotational speed of 30,000–60,000 rpm have found wide application as a gyro-motor for spinning the gyroscope. In autonomous power engineering, high-speed EMs are developed as a microturbine component. Elliott Group serially produces decentralized power plants with 68,000-rpm magnetoelectric generators [8]. Capstone produces microturbines with high-speed magnetoelectric generators. A distinctive feature of these generators is that the rotor is installed on two air bearings, and the third air bearing is located between the compressor and turbine working wheels [9].

In decentralized energy, the high-speed EMs have found a wide industrial application. Their development is aimed to reduce bearing losses, to increase the working temperature and efficiency. In addition, the high-speed EMs with a power below 250 kW find application in the power supply systems of aircrafts and space vehicles. There are two main variants of high-speed EMs for aircrafts: switched-reluctance EM and EM with HCPM. Comparison of these EM types is presented in different works. It is shown that the high-speed EMs with HCPM have smaller mass-and-size parameters than in switched-reluctance EMs. This determines their preferred use in aircrafts.

The development of such industries as robotics, machine tool, turbomolecular pumps, high-tech medical equipment, etc. and the development of new-generation unmanned aircraft require the creation of ultra-high-speed EMs with a rotational speed from 200,000 to 1,000,000 rpm or more and a power from 50 W to 2 kW [10]. The main advantage of this EM type is a high power density with overall miniature dimensions, which causes wide prospects for their use in various microsystems. In addition, a significant advantage of ultra-high-speed EMs is the uniqueness of the tasks they solve. For example, the application of motor with a 400,000-rpm rotational speed in the machine tool improves the quality of surface treatment [11]. The 500-W microgenerator for an autonomous robotic complex allows abandoning battery cells that have high mass-and-size parameters. **Table 2** shows a comparison of various electricity sources for the electrical supply of robots.

With all the technical advantages of ultra-high-speed EMs with HCPM, this area began to develop relatively recently. The development of this area was facilitated by the emergence of

Electricity sources	Power-to-mass ratio [kW/kg]
Ultra-high-speed microgenerator with microturbine including the fuel mass	0.55
Batteries	0.50
Fuel cells	0.05
Ultra-high-speed microgenerator with flywheel system	0.50

Table 2. Comparison of various electricity sources for the electrical supply of robots.

new electrical materials and the development of microelectronics. Therefore, theoretical studies on this topic are limited and represent a disparate material, which describes individual design solutions for ultra-high-speed EMs for a particular application. It is necessary to consider the main development trends of this EM type and to consider in more detail examples of their practical application.

One of the application areas of ultra-high-speed EMs is autonomous system. Microturbines with ultra-high-speed EMs are planned to be used instead of storage batteries in robotic complexes, unmanned aerial vehicle, cryogenics, etc.

The main developers of ultra-high-speed EMs for microturbine installations are several countries: Japan (IHI Corporation), France (Onera), Switzerland (Power Electronic Systems Laboratory and ETH Zurich), USA, Germany (High-Speed Turbomaschinen GMBH). It seems advisable to consider their development in more detail.

Onera [12] (France, DecaWatt research program) developed a microturbine system with a microgenerator. The purpose of the program is the creation of a microturbine engine with a power of 50–100 W to provide electrical energy for ammunition and equipment for future soldiers. The microgenerator has a power of 55 W and a rotational speed of 840,000 rpm. The generator tests were performed at a rotational speed of 700,000 rpm. It was used in the mechanical high-speed bearings. The pole number of this high-speed EM is equal to 1. The frequency of the output voltage is 14,000 Hz. Ultra-high-speed EMs should be considered as a complex of interconnected systems, since the full efficiency of a high-speed EM and mass-and-size parameters are determined not only by material parameters and geometric dimensions of EM but also by parameters of its control system. In addition, a separate EM with an output frequency of 14 kHz without a power electronics unit is unlikely to find practical application. A similar conclusion was noted in [13, 14]. To achieve the maximum efficiency, Onera used the following technical solutions: amorphous magnetic materials (AMM) as a stator core material to minimize stator losses; a slotless stator design to simplify the manufacturing technology of the stator magnetic core, to reduce the inductance of the stator winding scattering and to minimize the demagnetizing effect of the armature reaction; and a cylindrical permanent magnet (PM) to simplify the rotor manufacturing technology.

According to a similar technology, Power Electronic Systems Laboratory and ETH Zurich developed and implemented two ultra-high-speed PM starter-generators for microturbines [15, 16]; one of which has a power of 500 W and a rotational speed of 500,000 rpm, and the second one has a power of 1 kW and a rotational speed of 500,000 rpm. To implement the ultra-high-speed EM, Power Electronic Systems Laboratory and ETH Zurich used the same technical

solutions as Onera. It was a slotless stator, a cylindrical PM and AMM were also used. For the implementation of the starter mode, sensorless control was used.

The same technical solutions are used by High Speed Turbomaschiner, which develops a 150-W high-speed magnetoelectric EM with a rotational speed of 490,000 rpm [17]. The stator magnetic core is slotless and made of AMM.

IHI Corporation developed a microturbine system with a microgenerator [18]. It contains an oil-free gas turbine with a 400-W ultra-high-speed magnetoelectric generator integrated into it. The rotational speed of the microgenerator is 400,000 rpm. Kerosene, propane, light oil, etc. can be used as fuel in the proposed system. Expected applications are power generation for charging portable devices and the use as a power source for robots.

Robot/Mechatronics Research Center [19] is working on the development of a microturbine with a 500-W microgenerator with a rotational speed of 400,000 rpm for unmanned aerial vehicles and robotic complexes. The stator of this generator is made with six slots in which a three-phase winding is laid. The rotor sleeve is made of Inconel 718 alloy. The HCPM type is $\text{Sm}_2\text{Co}_{17}$. The disadvantages of this generator are the slotted stator design, which considerably complicates the manufacturing technology of the stator magnetic core made of AMM. If the AMM is not used as a stator core material, the hysteresis losses in the stator magnetic core can significantly reduce the efficiency. For unmanned aerial vehicles and robotic complexes, Stanford University and MDOT Aeronautics develops an ultra-high-speed permanent-magnet EM with a power of 400 W and a rotational speed of 800,000 rpm [20].

For all the above-considered ultra-high-speed EMs for autonomous power supply systems, the shaft and the rotor back are made of nonmagnetic material to increase its mechanical strength. However, this leads to a decrease in its power and in the magnetic flux density in the EM air gap. Therefore, to increase the energy characteristics of ultra-high-speed EMs, it would be more expedient to use a magnetic material, for example, the cobalt alloy Vacodur S Plus, which is close to some titanium brands by its mechanical characteristics [1].

Thus, the ultra-high-speed EMs for autonomous power supply systems are actively developing abroad. They all practically have a common design: a slotless stator made of AMM and a rotor with cylindrical HCPMs.

The publication analysis shows that the research and optimization of the design of all the above-mentioned ultra-high-speed EMs was carried out together with power electronics and control systems [21]. The tendency to reduce number of manufactured parts in mechanical engineering by improving the quality of the treated surface poses the task of creating miniature machines and spindles of small power with ultra-high-speed EMs. In particular, [22] presents a design and prospects of using an ultra-high-speed EM with a 200,000-rpm rotational speed in machine tool to produce electronic components. The stator magnetic core is slotless and made of electrical steel 10SNEX 900 with a sheet thickness of 0.1 mm. The rotor speed is controlled by sensorless algorithms. The rotor sleeve is made of a carbon fiber.

Westwind [23] (United Kingdom) produces PCB spindles with ultra-high-speed EMs with rotational speeds from 85,000 to 370,000 rpm. All spindles are made with foil bearings. EMs with rotational speed of 370,000 rpm are used in a drilling machine to make holes with a

Parameter	Onera	ETH	Robot/mechatronics research center	Electric motor
EM type	PM generator	PM generator	PM generator	PM motor
Power [W]	55	1000	500	—
Rotational speed [rpm]	800,000	300,000–500,000	400,000	200,000
The need of a control system	Yes	Yes	Yes	Yes
Stator design	Slotless	Slotless	Slotted	Slotless
Stator magnetic core material	AMM	AMM	—	Electrical steel 10SNEX 900 with a sheet thickness of 0.1 mm

Table 3. Parameters of ultra-high-speed EMs.

diameter of 75 μm . In addition, ETH Zurich and Power Electronic Systems Laboratory [15] for the first time in the world developed a 100-W electrical motor with a rotational speed of 1,000,000 rpm, which was a breakthrough in rotational speeds of up to 1 million rpm. The electrical motor was made with HCPM and ceramic ball bearings.

One of the important applications of ultra-high-speed EMs is a high-tech medical equipment. Ultra-high-speed EMs are used in blood pumps, dental instruments, surgical operations, etc. For example, Sinotech Motors [24] developed the ultra-high-speed EMs for blood pumps. These motors are slotless. Their control system is integrated, which allows achieving minimum mass-and-size parameters. Sirona has developed the ultra-high-speed EMs for dental instruments [25]. EM data are executed with rotational speeds from 250,000 to 400,000 rpm. In [26], the design of an ultra-high-speed medicine pump based on the ultra-high-speed EM with a rotational speed of 200,000 to 600,000 rpm is described. The stator design of this EM is also slotless. In addition, sensorless control methods are used.

To analyze trends in the high-speed EMs, the EM parameters are listed in **Table 3**. It shows that all ultra-high-speed EMs are operated jointly with power electronics and control systems, which confirms the need to study them not as a separate electrical machine. In addition, all ultra-high-speed EMs have HCPMs, and their stators are slotless.

4. Efficiency of high-speed electrical machines

The EM efficiency is one of the main EM parameters and largely determines the EM design. For example, to increase the EM efficiency, slot skewing or contactless bearings are used, i.e., technical solutions that lead to the complication of the EM design and the production technology. Therefore, for the economic and technical justification of these complications, it is especially important to determine the EM losses and to select the effective EM design.

4.1. Winding losses in the high-speed EM

Total winding losses in the high-speed EM can be present as follow:

$$P_{\text{cu}} = P_{\text{m}} + P_{\text{ad}}, \quad (1)$$

where P_{m} is the winding losses and P_{ad} is additional eddy-current losses in winding.

Due to the uneven magnetization of the HCPM and the nonlinearity of loads, the current curve differs from the sinusoidal, i.e., the third, fifth, seventh spatial harmonics have appeared. In this case, the total winding losses are formed as the sum of the losses from these harmonics:

$$P_{\text{m}} = (I_1^2 + I_3^2 + I_5^2 + I_7^2)mr_a, \quad (2)$$

where I_1 is the first harmonic current, I_3 is the third harmonic current, I_5 is the fifth harmonic current, and I_7 is the seventh harmonic current.

To determine the eddy-current losses in winding, the following equation can be used:

$$P_{\text{ad}} = \frac{\pi^3 H_{\text{s max}}^2 \mu_0^2 f^2 d_s^4 \sigma_{\text{cu}} l_{\text{cu}}}{4}, \quad (3)$$

where $H_{\text{s max}}$ the maximum value of the magnetic field strength in the slot, f is the current frequency in the EM winding, d_s is the strand diameter, σ_{cu} is the specific electric conductivity of the winding, and l_{cu} is the total strand length.

The maximum value of the eddy-current losses in the winding is in the slotless EM design. For the slotted EMs, they are much smaller, but they also require calculation to determine and select the optimal cooling system. The most convenient calculation way is the computer simulation of the EM magnetic field and determination of the magnetic field crossing the winding in the slots. Analytical calculation methods are known, but they are cumbersome for engineering calculations.

4.2. Stator core losses of the high-speed EM

To determine the stator core losses in the EM, there is no general calculation methodology. In [27, 28], to determine the stator core losses in a wide frequency range, the following equation is proposed:

$$P_{\text{s.c}} = k_{\text{m}} P_{\text{s.c50/1}} \left(\frac{f}{50} \right)^{\beta} B^2, \quad (4)$$

where $P_{\text{s.c}}$ is the stator core losses [W/kg], $P_{\text{s.c50/1}}$ is the stator core losses at a 50 Hz frequency and a 1 T magnetic flux density, k_{m} is a coefficient of the increase in the stator core losses during processing, B is the magnetic flux density in the stator core, and $\beta = 1.3, \dots, 1.5$.

For a frequency of 400 Hz or more, the following equation [29, 30] is recommended for the stator core loss calculation:

$$P_{\text{s.c}} = P_{\text{sz}} + P_{\text{sj}} = k_{\text{m}} P_{\text{s.c.s}} B_j^2 M_j \left(\frac{f}{400} \right)^{1.5} + k_{\text{m}} P_{\text{s.c.s}} B_z^2 M_z \left(\frac{f}{400} \right)^{1.5}, \quad (5)$$

where $P_{s.c}$, P_{sz} , P_{sj} are stator core losses, losses in the stator teeth, and losses in the stator back, respectively; k_m is a coefficient that takes into account the increase in the stator core losses during processing; $P_{s.c.s}$ are stator core specific losses at a frequency of 50 Hz and a magnetic flux density of 1 T; B_j , M_j are the magnetic flux density and mass of the stator back, respectively; B_z , M_z are the magnetic flux density and mass of the stator teeth, respectively; f is the current frequency or magnetization reversal frequency of the stator back and teeth.

In [31], the following equation was proposed to determine the stator core losses:

$$P_{s.c} = (k_{hyst} B^\beta f + k_{eddy} B^2 f^2) M_s, \quad (6)$$

where $\beta = 1.7-2$; k_{gyst} , k_{vih} are hysteresis and eddy-current factors, respectively, and M_s is a stator mass.

A method for determining the stator core losses is proposed in [32], in which three coefficients characterizing the properties of the stator core material are used: the hysteresis loss coefficient k_{hyst} , the eddy-current loss coefficient k_{eddy} , and excess loss coefficient k_e :

$$P_{s.c} = k_{hyst} B^2 f + k_{eddy} B^2 f^2 + k_e (Bf)^{\frac{3}{2}}. \quad (7)$$

These coefficients are often indicated by manufacturers of electrotechnical steels and soft magnetic alloys.

In [22], an empirical equation is presented for calculating the stator core losses of high-speed EM, which is the approximated dependence of the stator core losses on the current frequency of the 10JNEX900 steel:

$$P_{s.c} = (7 \cdot 10^{-4} B^{1.75} f^{1.5} + 4.7 \cdot 10^{-4} B^{1.86} f^{1.53}). \quad (8)$$

For analytical calculations of the stator core losses in the high-speed EMs in a wide frequency range, Eq. (5) is the most optimal. Coefficients of this equation should be determined based on the experimental studies or data of the specialized literature.

4.3. Influence of heating of EM with HCPM on specific losses in electrotechnical steels and precision soft magnetic alloys

During the operation of the EM with HCPM, their stator core will heat up under the influence of the ambient temperature, and because of the specific losses. An increase in the stator core temperature leads to a change in its magnetic properties. Therefore, it is necessary to evaluate the effect of the EM temperature on the stator core losses.

Measurements of the stator core losses were made under normal climatic conditions at sample temperatures below 23°C, relative air humidity of 25%, and at a temperature below 70°C. For studies at a temperature below 70°C, the sample was heated in a muffle furnace. Then, it was repeatedly measured in a cold state at a temperature below 23°C. Experimental studies have measured specific losses at different temperatures in two annular samples made of AMM (type

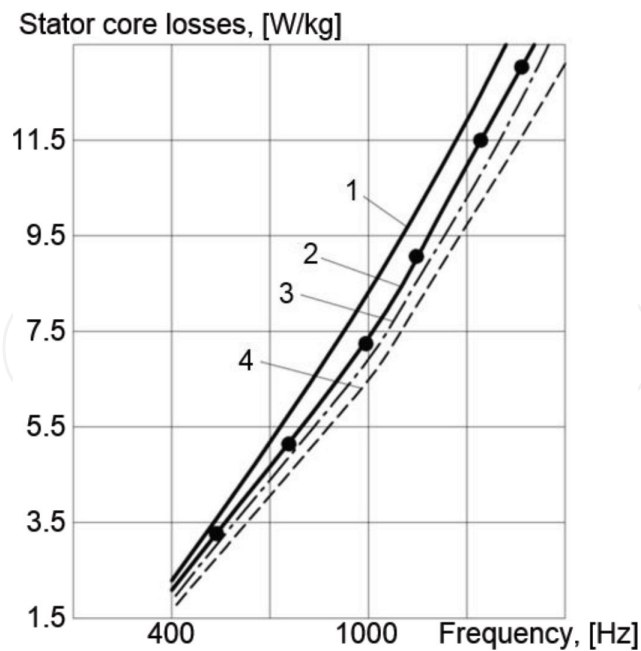


Figure 1. Dependence of the stator core losses on the frequency: curve 1 is for AMM, 5BCDR grade, type T at 20°C; curve 2 is for AMM, 5BCDR grade, type E at 20°C; curve 3 is for AMM, 5BCDR grade, type T at 70°C; and curve 4 is for AMM, 5BCDR grade, type E at 70°C.

E and type T of 5BDSR grade) produced by the Ashinsky metallurgical plant (Russia). The saturation magnetic flux density of these AMMs is 1.3 T. The experimental results at a magnetic flux density of 0.5 T are shown in **Figure 1**. It shows that with the temperature increase of the stator core made of AMM, 5BCDR grade, type T (linear hysteresis loop) to 50°C, the stator core losses decrease by 15%. For temperature increase of the stator core made of AMM, 5BCDR grade, type E (rectangular hysteresis loop) to 50°C, the stator core losses decrease by 14%. Thus, with the temperature increase of the stator core made of AMM, its losses decrease by 15%.

In addition to changing the losses in the EM stator core due to its heating, the losses in the EM stator core during operation will also decrease due to the decrease in the HCPM energy characteristics, and, accordingly, in magnetic flux density of the stator core. The study of this process will be given below. To assess this decrease, a computer model was developed in the Ansoft Maxwell software package, and a computer simulation for the magnetic field distribution along the section of the EM stator core was made. Simulation results for EM at a temperature of 23°C are presented in **Figure 2**. It was found that with an increase of the HCPM to 150°C, the magnetic flux density in the stator core decreases by 6–6.5%. Taking into account the dependence of the stator core losses on magnetic flux density for various materials, this can lead to reducing losses in the stator core by 13–15%. Thus, heating of the stator core leads to a significant loss reduction in the EM.

4.4. Eddy-current losses in the HCPM and rotor sleeve

In the high-speed EMs, spatial harmonics caused by the EM design, the winding type, or the distribution coefficient, as well as the time harmonics caused by an external circuit (for

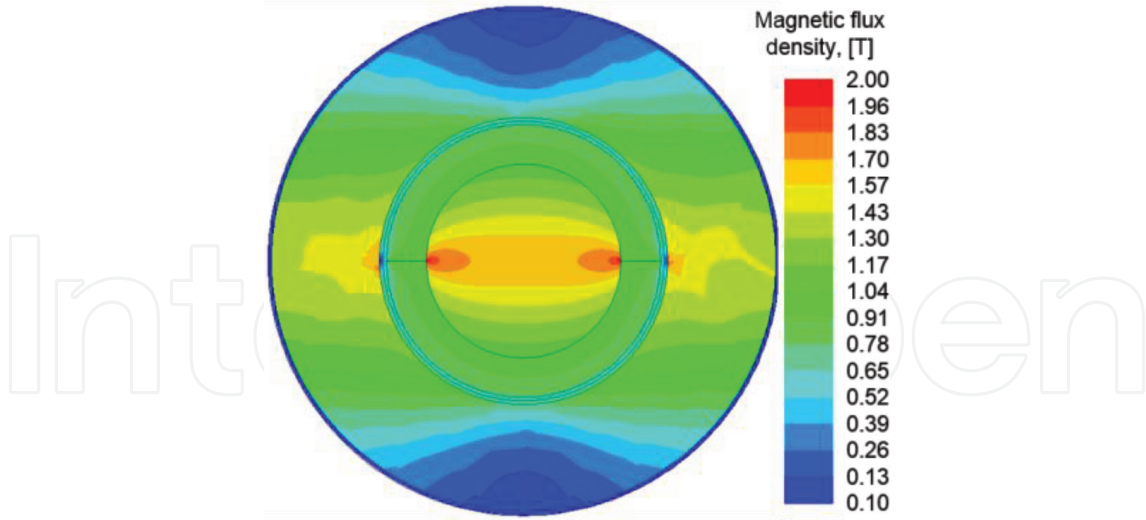


Figure 2. Simulation results for EM at a temperature of 23°C.

example, an inverter or rectifier) will induce significant eddy-current losses in the rotor sleeve or HCPM. This can lead to overheating of the HCPM and to demagnetization of the HCPM. To reduce these losses, HCPMs are usually laminated in the axial direction. To determine these losses, it is necessary to determine separately the losses due to time harmonics (external circuit) and losses due to spatial harmonics (EM design features). Usually, losses caused by time harmonics are greater than the losses caused by spatial harmonics. This statement is valid only for a number of the high-speed EM designs. For example, the EM with a tooth-coil winding has significant spatial harmonics, and losses caused by these harmonics are higher than the losses caused by time harmonics.

In the literature, there is no unambiguous opinion on the loss nature. Some authors argue that the losses in the HCPM are only due to eddy currents. At the same time, several authors argue that these losses are caused by eddy currents and magnetization reversal. In this chapter, the losses in the HCPM and rotor sleeve are considered as created only by eddy currents.

- a. Eddy-current losses in the HCPM and rotor sleeve created by time harmonics. As noted above, these losses are formed by an external circuit (rectifier or inverter), which are installed at the EM output for transmission to a standard frequency network. The EM calculation scheme is presented in **Figure 3**. To estimate these losses, expressions obtained by Poliender are convenient to use:

$$P_{\text{HCPM}} = \frac{r l h_m b_m^2}{12 \rho_m} \left\{ \left\{ (p a_m + \sin(p a_m)) \left(\frac{d}{dt} (\hat{B} \cos(p \beta)) \right) \right\}^2 + \left\{ (p a_m - \sin(p a_m)) \left(\frac{d}{dt} (\hat{B} \cos(p \beta)) \right) \right\}^2 \right\} \quad (9)$$

where p is a number of pole pairs, l is the HCPM length, h_m is the HCPM height, ρ_m is the HCPM resistivity, r is an average air gap radius, a_m is a pole angle, b_m is a pole arc length, and \hat{B} is a magnetic flux density created by time harmonics.

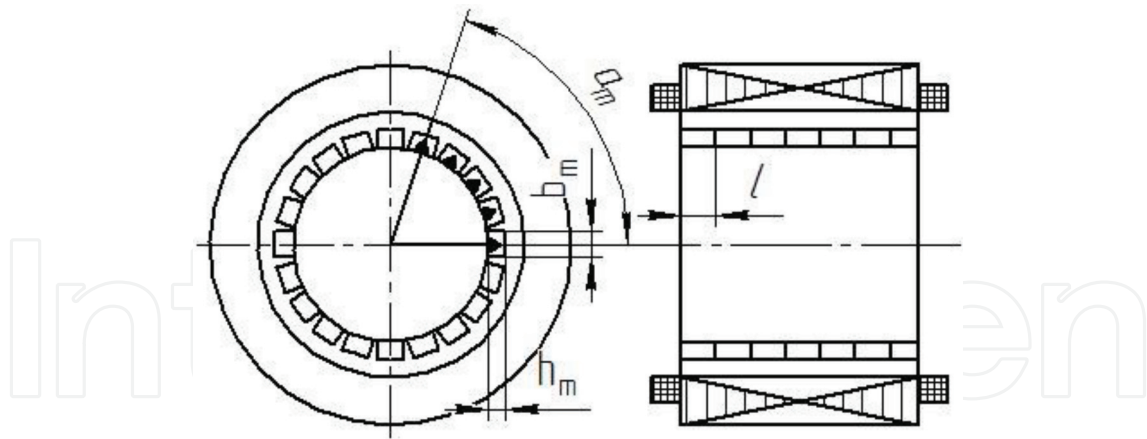


Figure 3. EM calculation scheme.

To determine the magnetic flux density produced by time harmonics, it is necessary to understand the time harmonics magnitude produced by different types of nonlinear load in the EM windings. To solve this problem, a simulation EM model with an external network was developed in the LTSpice IV. It contains a three-phase EM with HCPM, an uncontrolled rectifier, and a DC load (**Figure 4**). The EM was represented by three single-phase sources and three pairs of magnetically coupled inductors forming a three-phase voltage.

Simulation was carried out for a system with a three-phase 115/200 V source (EM with HCPM) with a frequency of 400 Hz, a grounded neutral and a load connected via a single-phase or a three-phase rectifier. In **Figures 5** and **6**, the simulated circuits for the inclusion of three-phase and single-phase nonlinear loads are presented. As a simulation result, the current and voltage curves of the EM and the load are shown in **Figures 7–14**.

To simplify the comparative analysis and to determine the influence of a certain nonlinear load inclusion scheme, the obtained data were summarized in **Table 4**. It shows that when a three-phase rectifier is connected, the phase current of the EM with the HCPM contains spatial harmonics with the numbers 5, 7, 11, 13, 17, 19 in addition to the fundamental harmonic.

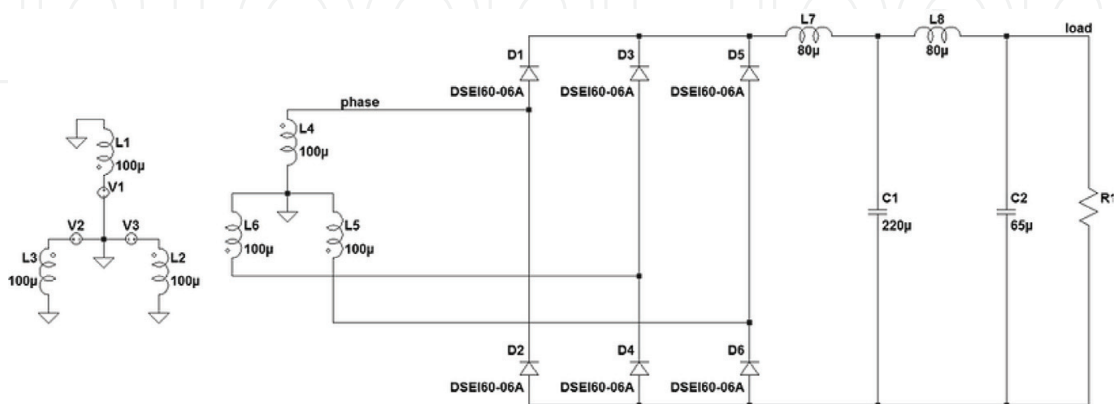


Figure 4. EM simulation model with external network for determining time harmonics and losses generated by them.

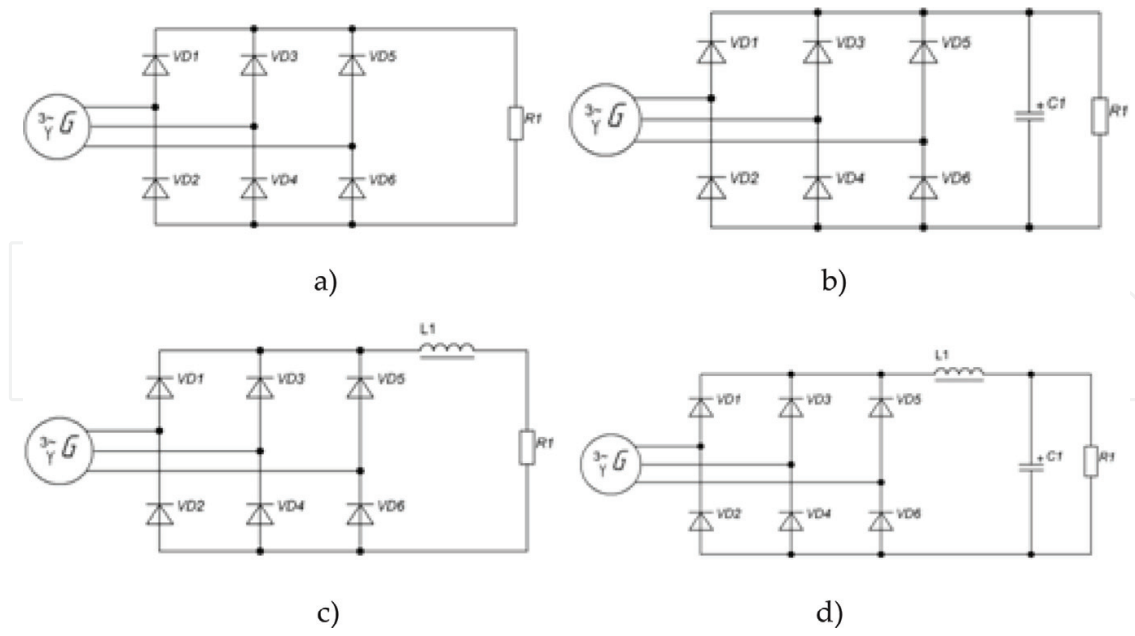


Figure 5. The simulated circuits for the inclusion of three-phase nonlinear loads: (a) active load, (b) active-capacitive load, (c) active-inductive load, and (d) active-inductive-capacitive load.

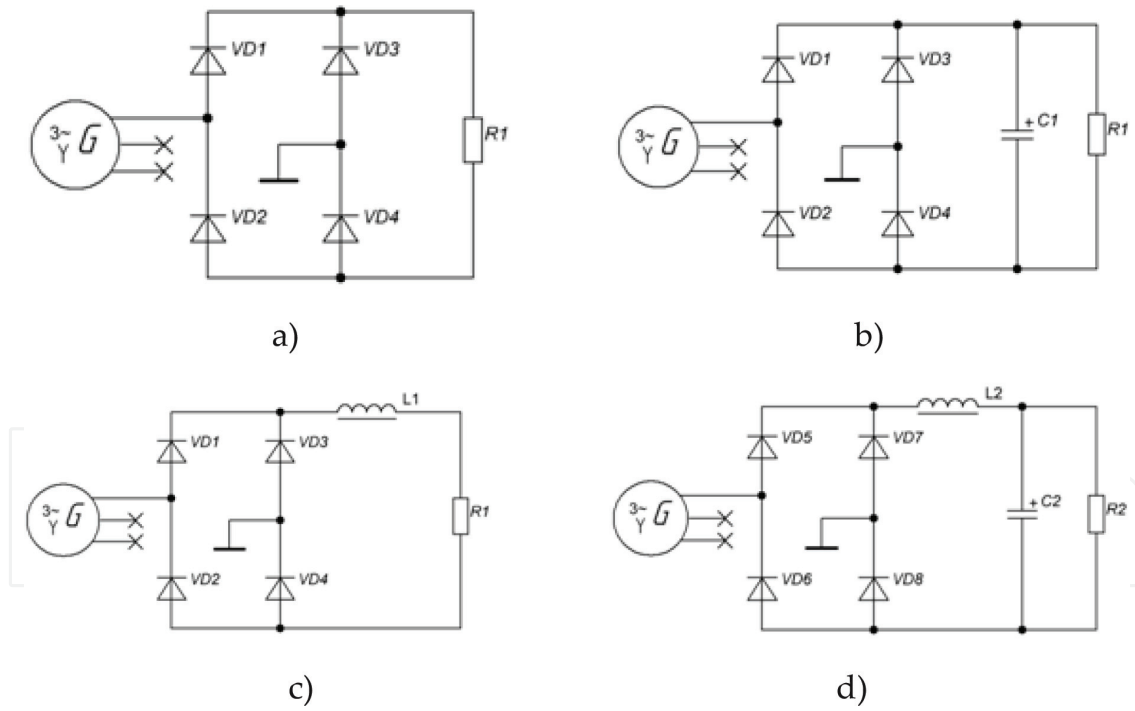


Figure 6. The simulated circuits for the inclusion of single-phase nonlinear loads: (a) active load, (b) active-capacitive load, (c) active-inductive load, and (d) active-inductive-capacitive load.

Harmonics that are multiples of three are absent. For the studied numerical parameters, the worst case scenario is for a three-phase active-capacitive load and a single-phase active-capacitive load. In this case, the harmonic coefficient reaches 95.2%. For an active nonlinear

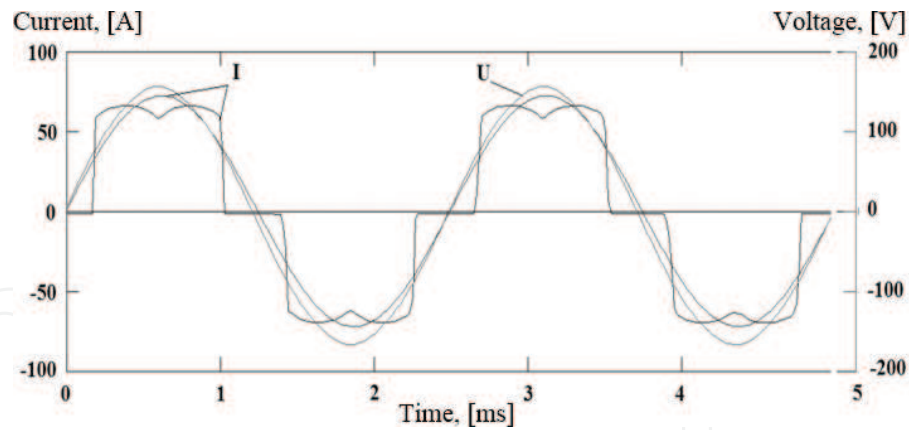


Figure 7. Curves of the voltage, total current, and fundamental current harmonic for the circuit in Figure 5a.

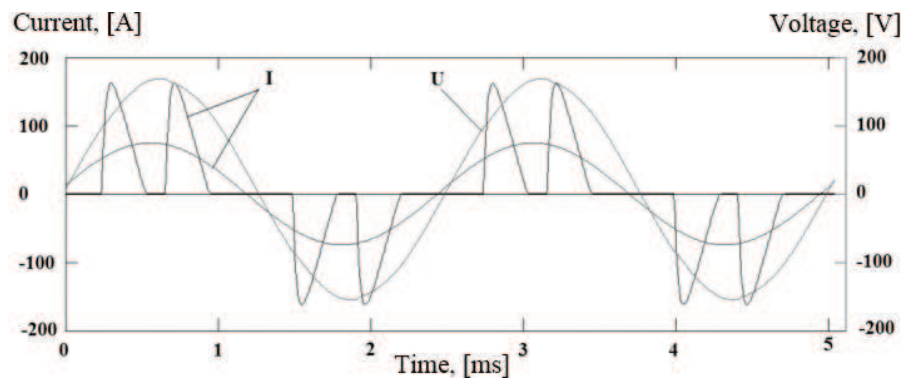


Figure 8. Curves of the voltage, total current, and fundamental current harmonic for the circuit in Figure 5b.

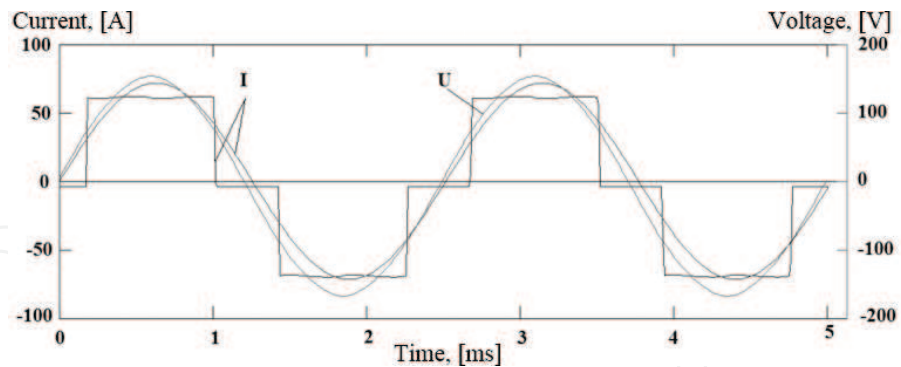


Figure 9. Curves of the voltage, total current, and fundamental current harmonic for the circuit in Figure 5c.

three-phase load, the total harmonic distortion (THD) is 29%. For an active-inductive nonlinear load, the THD is 31.1%. It is obvious that the voltage harmonic composition of the EM with nonlinear load characterizes the harmonic composition of the magnetic flux density created by the time harmonics.

To confirm the computer simulation data, an experimental setup was developed. It consists of a DC motor with independent excitation, EM, pulse width modulation (PWM) controller of the

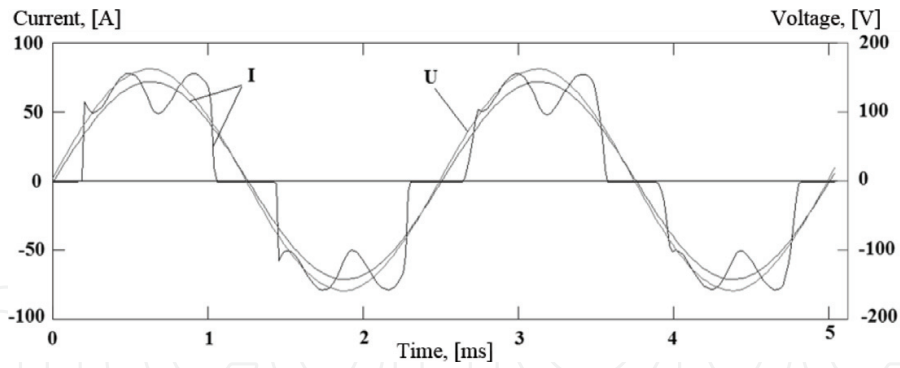


Figure 10. Curves of the voltage, total current, and fundamental current harmonic for the circuit in Figure 5d.

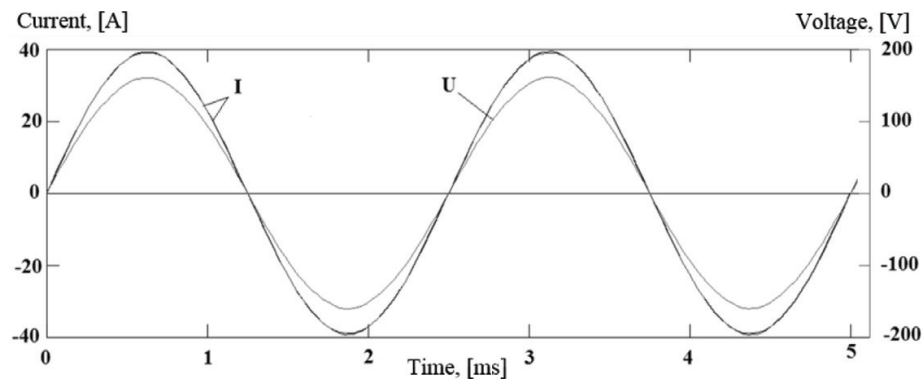


Figure 11. Curves of the voltage, total current, and fundamental current harmonic for the circuit in Figure 6a.

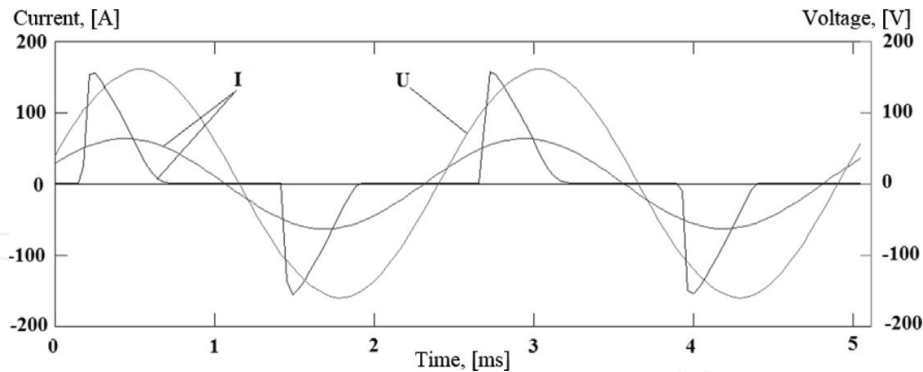


Figure 12. Curves of the voltage, total current, and fundamental current harmonic for the circuit in Figure 6b.

rotational speed for the DC motor, and rectifier with an active load. The PWM controller sets the rotational speed of DC motor, which the armature winding is connected to the PWM controller. The excitation winding is supplied from a constant current source with a voltage of 27 V and a current of 2 A. The PWM controller is powered by a 27 V DC source with a current of 15 A. The DC shaft is mechanically connected to the EM shaft. The rotational speed of EM is 8000 rpm, the output voltage is 36 V, and the output current is 3.2 A. The outputs of the EM

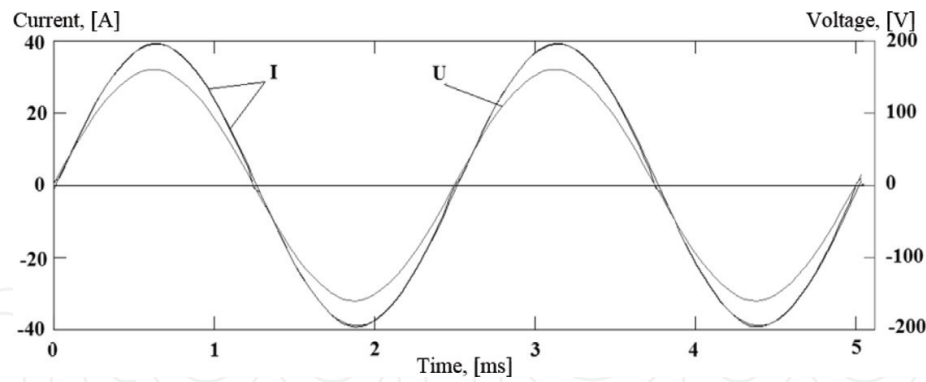


Figure 13. Curves of the voltage, total current, and fundamental current harmonic for the circuit in **Figure 6c**.

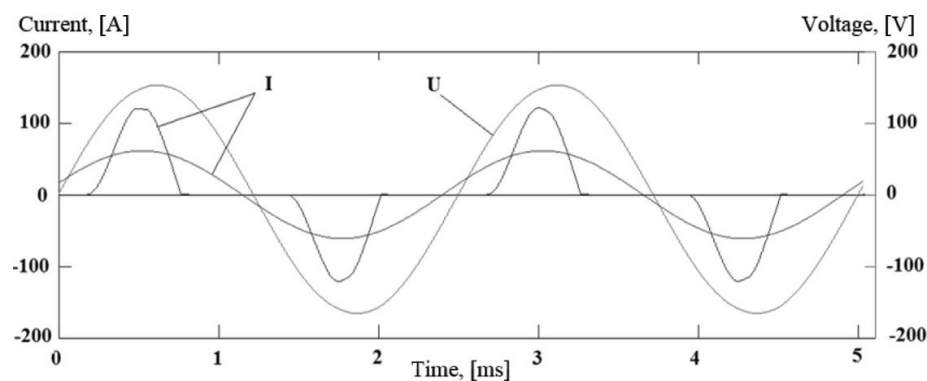


Figure 14. Curves of the voltage, total current, and fundamental current harmonic for the circuit in **Figure 6d**.

Scheme	Total power [kVA]	Power [kW]	$\cos \varphi$	$\cos \varphi(1)$	THD [%]
Three-phase active load	18.0	17.3	0.96	1.00	29.0
Three-phase active-capacitive load	24.7	17.5	0.71	0.99	95.2
Three-phase active-inductive load	17.9	17.1	0.95	1.00	31.3
Three-phase active-inductive-capacitive load	18.0	17.1	0.95	1.00	31.7
Single-phase active load	3.1	3.1	1.00	1.00	2.4
Single-phase active-capacitive load	6.9	4.5	0.65	0.90	93.3
Single-phase active-inductive load	3.1	3.1	1.00	1.00	3.6
Single-phase active-inductive-capacitive load	6.2	4.7	0.76	0.97	76.9

Table 4. Comparison of simulation results of connection schemes.

stator winding through a three-phase rectifier are connected to a resistive load of 100 W with the LTS-6NP-type series-connected current transformers.

The experimental results correspond to the simulation data, which indicate the adequacy of the developed simulation model and the obtained theoretical results: the frequency of the fundamental harmonic is 396 Hz, THD is 29.6%, $\cos \varphi = 0.95$, and $\cos \varphi(1) = 1.0$.

In addition, it is possible to determine the losses in the HCPM and rotor sleeve by using the obtained data. For example, calculations were made for EM with rotational speeds of 5000 and 32,000 rpm at active-inductive load. It was found that for nonlaminated HCPM, the eddy-current losses are above 280 W at a frequency of 5000 rpm and above 8 W at a frequency of 32,000 rpm.

- a. Eddy-current losses in the HCPM and rotor sleeve created by spatial harmonics. These losses are determined by the slot type, the slot size, and the winding type; i.e., it depends on many different factors. Analytically, the definition of these losses is difficult and does not give the necessary accuracy. Therefore, it is more expedient to use the finite element method (FEM) to analyze the losses in the HCPM and rotor sleeve.

To solve this task in Ansys Maxwell software package, it is necessary to specify the specific HCPM conductivity. It is 1,100,000 S/m for SmCo and 625,000 S/m for NdFeB. In the project window, in the excitation section, the eddy-current calculation (Set Eddy Effects) is carried out, and HCPM and the rotor sleeve are selected. In a simulation result, the distribution of eddy-current losses in the HCPM and rotor sleeve on the spatial harmonics will be obtained in the Fields Overlaps-Field-Ohmic_loss tab. **Figures 15–17** show the distribution of the magnetic field and the eddy-current losses in the HCPM caused by spatial harmonics for 250-kW 60,000-rpm EMs with a distributed winding, a tooth-coil winding, and a slotless design. The number of pole pairs for all considered EMs was equal to 4. In addition, the minimum eddy-current losses in the HCPM caused by spatial harmonics have the slotless EM and the EM with a distributed winding. The maximum eddy-current has the EM with a tooth-coil winding. The difference between the losses in EM with distributed and tooth-coil winding is above 500%. Therefore, it is obvious that in the high-speed EMs with a tooth-coil winding, the eddy-current losses in the HCPM caused by spatial harmonics exceed the eddy-current losses in the HCPM and the rotor sleeve caused by time harmonics.

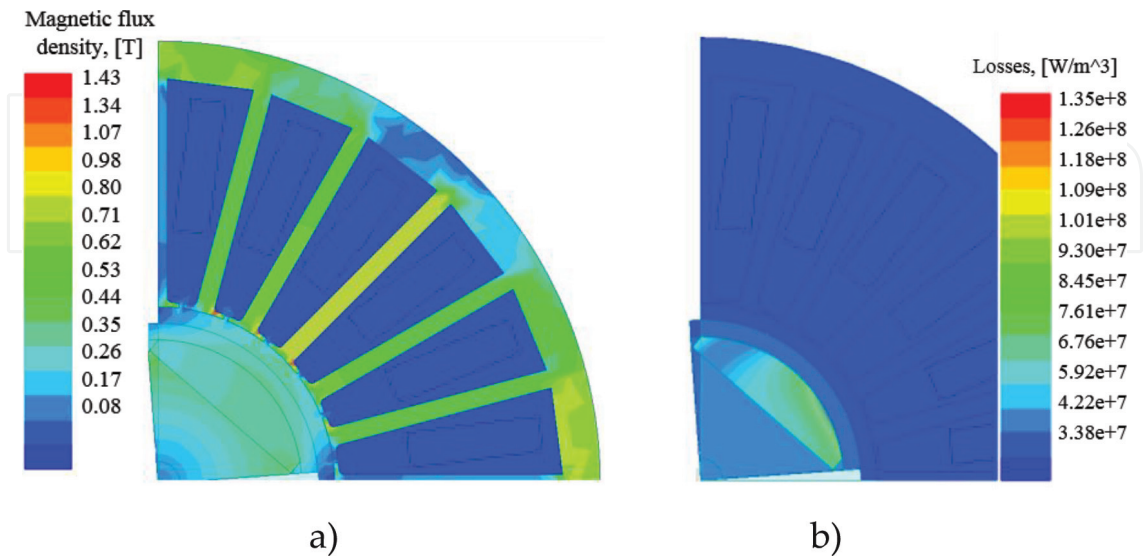


Figure 15. Distribution of the magnetic field (a) and the eddy-current losses (b) in the HCPM of the slotless EM with a distributed winding.

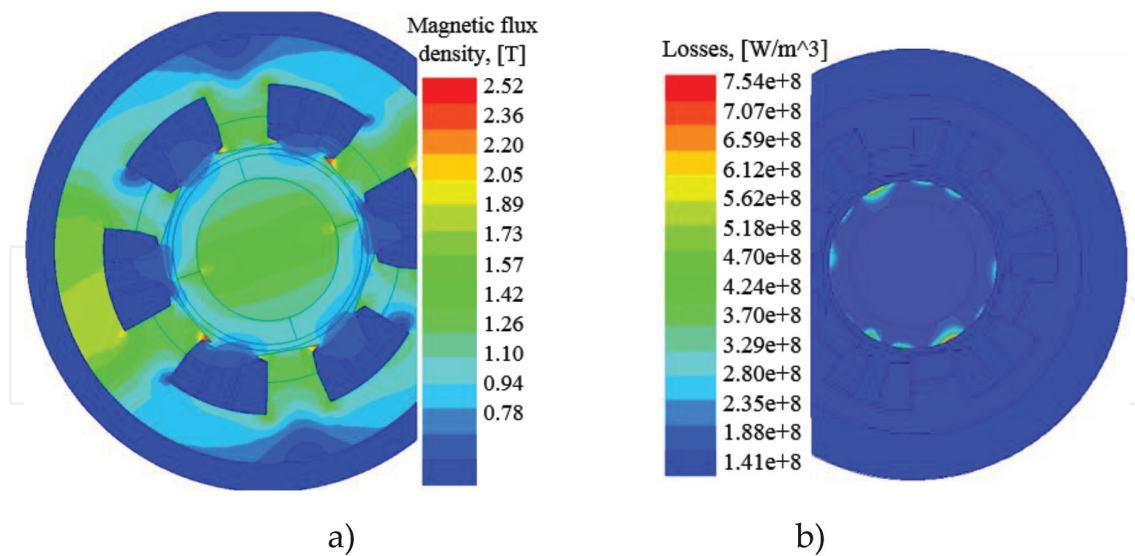


Figure 16. Distribution of the magnetic field and the eddy-current losses in the HCPM of the slotless EM with a tooth-coil winding.

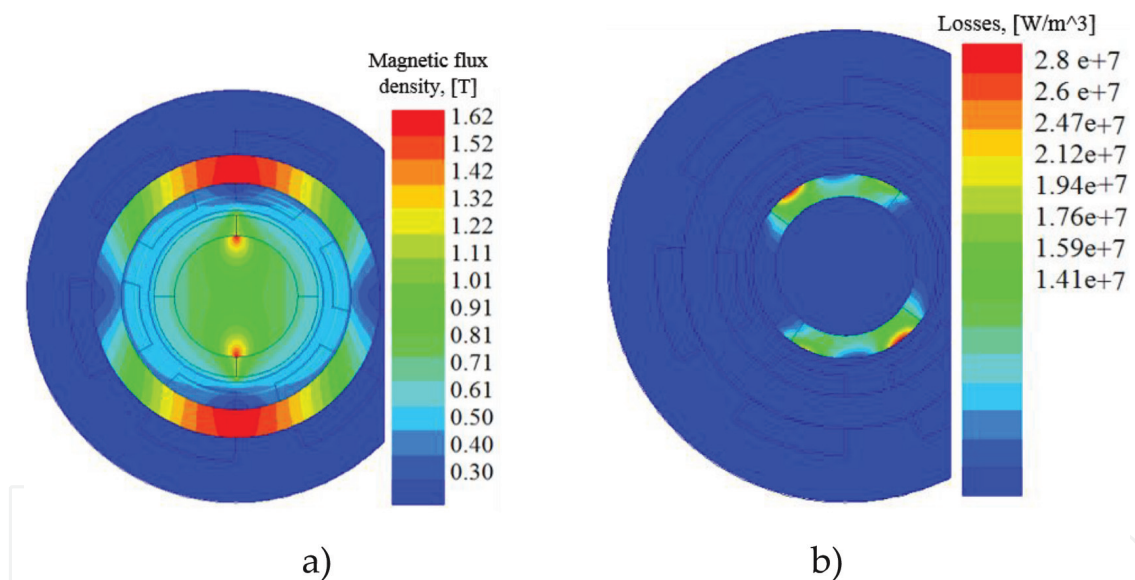


Figure 17. Distribution of the magnetic field (a) and the eddy-current losses (b) in the HCPM of the slotless EM.

In addition, it seems advisable to estimate the influence of the rotor magnetic system (MS) type on the eddy-current losses of HCPM in the high-speed EM.

This task was also solved by computer simulation methods. The results are shown in **Figure 18**. It can be seen that the MS type does not significantly affect the HCPM losses. This is explained by the fact that the HCPM losses are formed by the stator magnetic field. In the case of a constant slot zone, the stator magnetic field remains unchanged. With an increase in the rotational speed, the HCPM losses have a maximum point, after which they begin to decrease. This is because with rotational speed increase, the magnetic field penetration depth in the

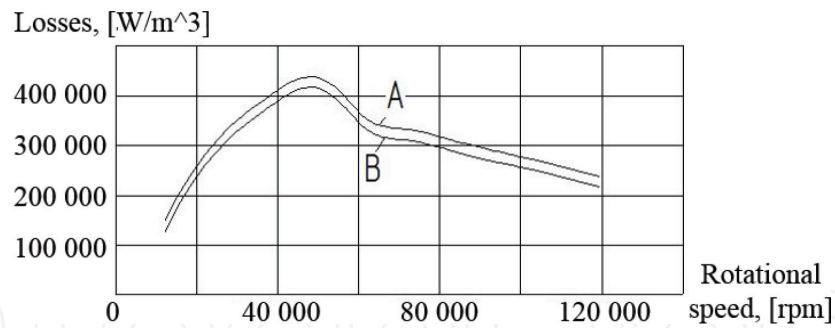


Figure 18. Dependence of eddy-current losses in the HCPM on the frequency and MS type: A—MS with cylindrical HCPM and B—MS with semicircular HCPM.

HCPM and rotor sleeve is reduced, and thereby the losses are reduced. Thus, the MS type has no significant effect. The eddy-current losses in the HCPM can vary considerably due to the change in the load angle. This should be taken into account in the design of the EM with HCPM.

The reduction of the eddy-current losses in the HCPM and rotor sleeve of the high-speed EMs can be achieved by the following ways.

For losses created by time harmonics:

- increasing the number of phases and thereby reducing pulsations,
- lamination of the HCPM and rotor sleeve in the axial direction,
- increasing the air gap and reducing the magnetic field penetration depth into the HCPM and the rotor sleeve.

For losses created by spatial harmonics:

- slot skewing and the selection of a large winding distribution coefficient,
- lamination of the HCPM and rotor sleeve in the axial direction,
- increasing the air gap and reducing the magnetic field penetration depth into the HCPM and the rotor sleeve.

For the EM with a tooth-coil winding, the minimization of the eddy-current losses created by spatial harmonics can be achieved by the correct selection of the number of stator slots and the number of rotor poles.

4.5. Eddy-current losses in bearings of the high-speed EM

For limited axial dimensions of the EM rotor and insignificant bearing removal from the HCPM in the high-speed EM, the bearing balls can be magnetized under the influence of the HCPM stray magnetic field. In a result, eddy currents are induced. This leads to overheating of the bearing caused by its hysteresis losses. With increase in the rotational speed, the overheating increases significantly. Therefore, the study of these processes is important for the high-speed EMs.

The magnitude of the magnetic field flowing through the bearing is determined by the bearing removal from the HCPM. For a numerical evaluation, a computer simulation of the three-dimensional magnetic field of the EM with HCPM was performed. The results of this simulation are presented in **Figure 19**. It shows that the magnetic flux density is 0.32 T at a distance from HCPM. That is quite a sufficient value for the magnetization of the bearing balls and the appearance of eddy-current losses in the bearing.

The object of study is the EM with HCPM. The geometric dimensions of the rotor are shown in **Figure 20**. The shaft is made of steel with a saturation magnetic flux density of 1.7 T. In this case, the effective value of magnetic flux density in the rotor steel is close to saturation (1.6–1.65 T).

The following assumptions are used:

- the magnetic permeability of the environment and air gap is equal to the magnetic permeability of the vacuum; and the magnetic permeability of the magnetic core, shaft, and bearings are equal to infinity;
- the stator winding is represented as a thin electrically conductive layer distributed along the stator core diameter;
- the density of the induced currents along the winding and bearing is constant;
- the mutual influence of temperature and magnetic fields is not taken into account;
- the influence of winding ends on the ball bearing magnetization is not taken into account.

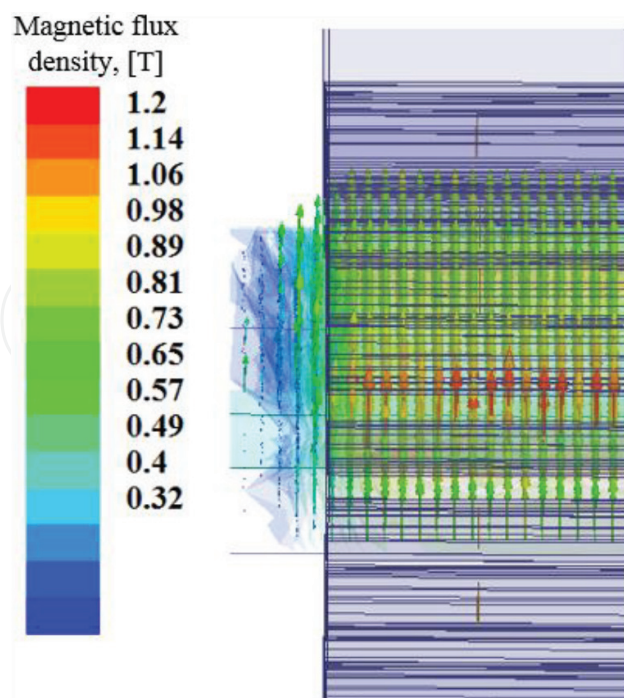


Figure 19. The three-dimensional magnetic field of the EM with HCPM.

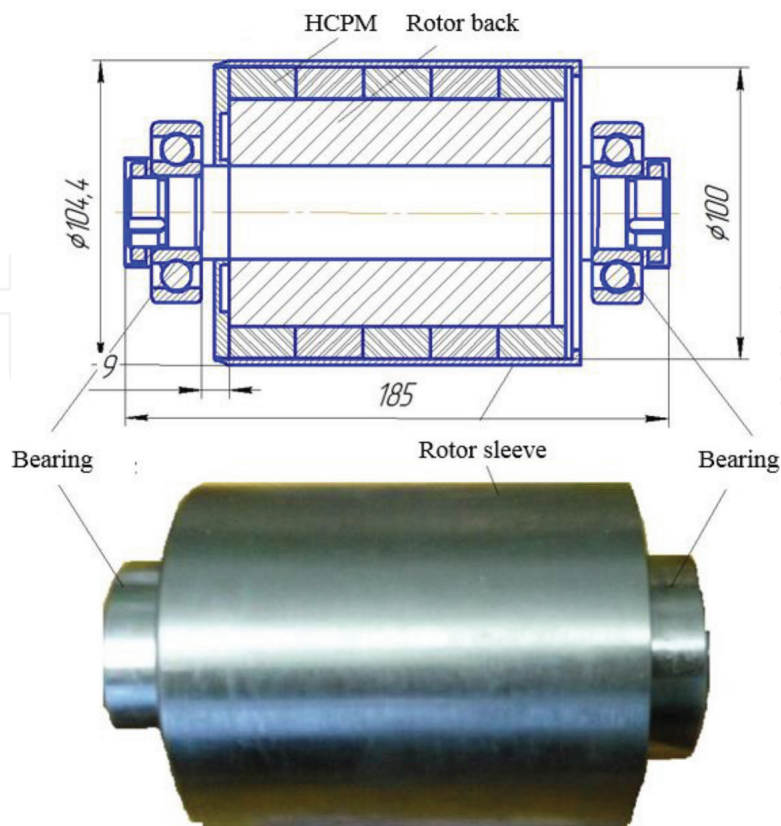


Figure 20. Calculation and experimental models of the research object.

To develop analytical equations for the loss analysis in the bearing, the EM calculation scheme presented in Figure 21 is considered.

The mathematical analysis of eddy-current losses includes the determination of the three magnetic field components of the EM with the finite-length HCPM. Maxwell’s equations are considered here:

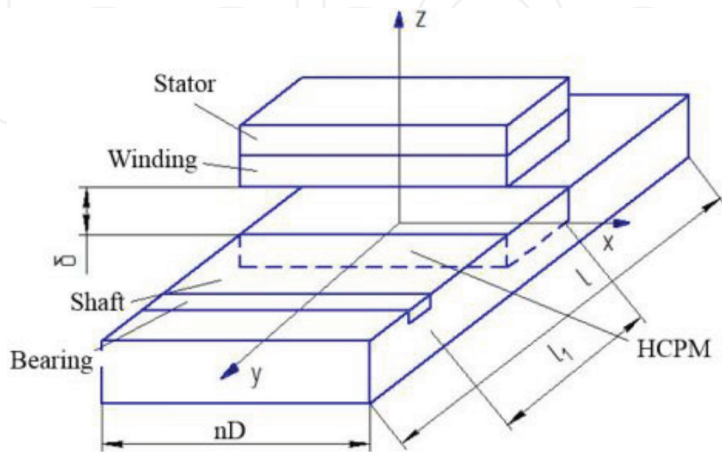


Figure 21. The EM calculation scheme.

$$\text{rot} \vec{H} = \vec{j} + \vec{j}_{\text{ex}}, \text{rot} \vec{E} = -\frac{\partial \vec{B}}{\partial t}, \vec{j} = \sigma [\vec{E} + (\vec{V} \times \vec{B})], \text{div} \vec{B} = 0, \text{div} \vec{j} = 0, \vec{H} = \mu_0 \vec{B} \quad (10)$$

where \vec{B} is a magnetic flux density vector, \vec{E} , \vec{H} are vectors of electric and magnetic fields, respectively, \vec{V} is a rotor velocity vector, σ is an electric conductivity of the stator winding, \vec{j} is an induced current density vector, and \vec{j}_{ex} is an external current density vector.

Since there are no currents in the air gap δ , the magnetic field in the air gap is described by the Laplace's equation in partial derivatives:

$$\Delta \vec{H} = 0, \frac{\partial^2 H_z}{\partial z^2} + \frac{\partial^2 H_z}{\partial x^2} + \frac{\partial^2 H_z}{\partial y^2} = 0, \frac{\partial^2 H_x}{\partial z^2} + \frac{\partial^2 H_x}{\partial x^2} + \frac{\partial^2 H_x}{\partial y^2} = 0, \frac{\partial^2 H_y}{\partial z^2} + \frac{\partial^2 H_y}{\partial x^2} + \frac{\partial^2 H_y}{\partial y^2} = 0. \quad (11)$$

The components H_x , H_y , H_z provide the continuity conditions of the magnetic field lines, while H_z provides the energy conversion.

The magnetic field on the HCPM surface is given as a normal tension component:

$$H_{z0} = H_{z0} \cos q_1 x \cos q_2 y, \quad (12)$$

where $q_1 = \frac{\pi}{\tau}$, $q_2 = \frac{\pi}{l}$, $q_3 = \sqrt{q_1^2 + q_2^2}$, τ is a pole pitch, l is a rotor length, and H_{z0} is a function of coercive force and residual magnetic flux density and is determined by their magnetization.

The mathematical description of HCPM is represented as a dependence of the coercive force, residual magnetic flux density, and magnetization:

$$\vec{B} = \mu \mu_0 (\vec{M} + \vec{H}), \quad (13)$$

where \vec{M} is the HCPM magnetization vector and μ is the HCPM magnetic permeability.

The solution of Laplace's equations is sought in the form:

$$\begin{aligned} H_z &= (C_1 \text{sh} q_3 z + C_2 \text{ch} q_3 z) \cos q_1 x \cos q_2 y, \\ H_x &= (C_3 \text{sh} q_3 z + C_4 \text{ch} q_3 z) \sin q_1 x \cos q_2 y, \\ H_y &= (C_3 \text{sh} q_3 z + C_4 \text{ch} q_3 z) \cos q_1 x \sin q_2 y. \end{aligned} \quad (14)$$

The initial conditions determine the integration constants:

1. $z = 0$
2. $z = \delta$, $y C_1 \text{ch} q_3 \delta + y C_2 \text{sh} q_3 \delta = 0$, $C_1 = -C_2 \text{th} q_3 \delta$;
3. $\text{div} H = \frac{\partial H_z}{\partial z} + \frac{\partial H_x}{\partial x} + \frac{\partial H_y}{\partial y} = 0$ —magnetic field continuity conditions.

Then:

$$H_z = q_3 (C_1 \text{sh} q_3 z + C_2 \text{ch} q_3 z) \cos q_1 x \cos q_2 y + q_1 (C_3 \text{sh} q_3 z + C_4 \text{ch} q_3 z) \cos q_1 x \cos q_2 y + q_2 (C_3 \text{sh} q_3 z + C_4 \text{ch} q_3 z) \cos q_1 x \cos q_2 y. \quad (15)$$

Equal terms can be obtained for the same functions sh and ch:

$$q_3 C_1 + q_1 C_4 + q_2 C_4 = 0, q_3 C_2 + q_1 C_3 + q_2 C_3 = 0. \quad (16)$$

Hence, the following is obtained:

$$C_4 = -C_1 \frac{q_3}{q_1 + q_2}, C_3 = -C_2 \frac{q_3}{q_1 + q_2} = -C_2 \frac{\sqrt{q_1^2 + q_2^2}}{q_1 + q_2}.$$

Taking into account the relations for C_1, C_2, C_3, C_4 , the components of the three field strength vectors have the form:

$$\begin{aligned} H_z &= H_{z0m} (\text{ch} q_3 z - \text{th} q_3 \delta \text{sh} q_3 z) \cos q_1 x \cos q_2 y, \\ H_x &= -H_{z0m} \frac{q_3}{q_1 + q_2} \text{ch} q_3 z (\text{th} q_3 \delta - \text{th} q_3 z) \sin q_1 x \cos q_2 y, \\ H_y &= -H_{z0m} \frac{q_3}{q_1 + q_2} \text{ch} q_3 z (\text{th} q_3 \delta - \text{th} q_3 z) \cos q_1 x \sin q_2 y. \end{aligned} \quad (17)$$

It is obvious that the component H_z is the primary magnetic field for the rotating bearing balls at $l = l_1$. This component magnetizes the bearing balls and induces eddy-currents in the bearing. In this case, the bearing is represented as an EM. It is assumed that the pole number of a given EM is equal to the number of bearing balls (**Figure 22**). The air gap in this case tends to zero. It should be noticed that the process of the ball magnetization has a complex character, taking into account possible interactions between neighboring balls, and the pole number of the EM cannot be equal to the number of bearing balls.

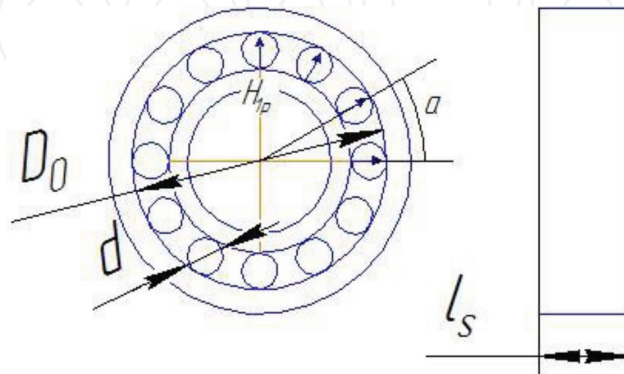


Figure 22. Calculation scheme of the bearing.

The resulting bearing magnetic field can be represented by the sum of two magnetic fields: bearing ball field and bearing cage field: $\vec{H} = \vec{H}_1 + \vec{H}_2$ and $\vec{B} = \vec{B}_1 + \vec{B}_2$.

The system of Maxwell's equations for the bearing is presented as:

$$\text{rot } \vec{H} = \vec{j} + \vec{j}_{\text{ex}}; \text{rot } \vec{E} = -\frac{\partial \vec{B}_1}{\partial t} - \frac{\partial \vec{B}_2}{\partial t}; \vec{j} = \sigma \left[\vec{E} + (\vec{V} \times \vec{B}) \right]; \text{div } \vec{B} = 0, \text{div } \vec{j} = 0; \vec{H} = \mu_0 \vec{B}. \quad (18)$$

The field on the bearing ball surface (primary field) is presented as following:

$$H_{1p} = H_{z0m} (\text{ch} q_3 D_0 - \text{th} q_3 \delta \text{sh} q_3 D_0) \cos q_1 x \cos q_2 l_1. \quad (19)$$

Solving the system of Maxwell's equations concerning the intensity of the secondary field, there is the following:

$$\Delta \vec{H}_2 - \mu_0 \sigma \left(d \frac{d \vec{H}_2}{dt} - \text{rot} (\vec{V} \times \vec{H}_2) \right) = -\mu_0 \sigma \left(d \frac{d \vec{H}_1}{dt} - \text{rot} (\vec{V} \times \vec{H}_1) \right). \quad (20)$$

The final solution of this system is not given here. The losses in the bearing cage are determined based on that $j_{2y} = -\frac{\partial H_{2z}}{\partial x}$.

Losses in the bearing cage are defined as $P = j_{2y}^2 / \sigma_s$, where σ_s is the conductivity of the bearing cage material. Since the bearing is represented as an EM, the bearing cage field will create a demagnetizing reaction (armature reaction) that can demagnetize the bearing balls and induce eddy currents in the bearing balls. By analogy of the eddy-current losses in the EM with the HCPM, eddy-current losses can be defined as:

$$P_{\text{sh}} = l_s d^2 \sum_{n=1}^n \frac{d^2}{12\rho} \left(\frac{d}{dt} \{ B_2 \cos(p(a - \beta)) \} \right)^2. \quad (21)$$

where ρ is a specific resistance of the bearing cage material, d is a bearing ball diameter, and p is the number of pole pairs of the EM, which is equivalent to the bearing.

The developed mathematical equations provide a general understanding of the loss occurrence processes in the bearing cage. They are obtained with a variety of assumptions, and the main one is that the number of poles is equal to the number of bearing balls. Therefore, the developed mathematical apparatus can be used for preliminary loss calculations in bearings and the selection of their location on the shaft of the EM with the HCPM.

4.6. Winding losses in the high-speed EMs

In addition to energy losses in the stator windings and stator core, windage losses are important to determine the efficiency of high-speed EMs with slotted and slotless stator design.

Winding loss analysis is considered in different works. In [29], the model proposed takes into account the effect of environmental pressure on the windage losses. Another model proposed in [33] describes the winding losses that are analogous to the model proposed by M. Mack, which has experimental confirmation to use in the EM. In this model, winding losses are determined by the equation:

$$P_f = c_f \pi \rho_{\text{air}} \Omega^3 R_r^4 l, \quad (22)$$

where c_f is a friction coefficient between rotor end environment, ρ_{air} is an air density, R_r is a rotor radius, Ω is a rotational speed [rad/s], and l is a length of the site on which losses are determined.

This model does not take into account the windage loss dependence on the environment pressure, the air gap temperature, and the stator and rotor slots, for example in the induction EMs. Analysis of Eq. (7) shows that the winding losses depend to the rotational speed. Consequently, the negligence of the air gap temperature, pressure and structural features of the stator, and rotor can cause errors in calculations and can also lead to incorrect selection of the rotor design and to decrease the efficiency of the high-speed EM.

Thus, this model needs refinements. For this, two designs are considered: EM with a smooth rotor and a slotted stator and EM with a slotted rotor and a slotted stator (**Figure 23**).

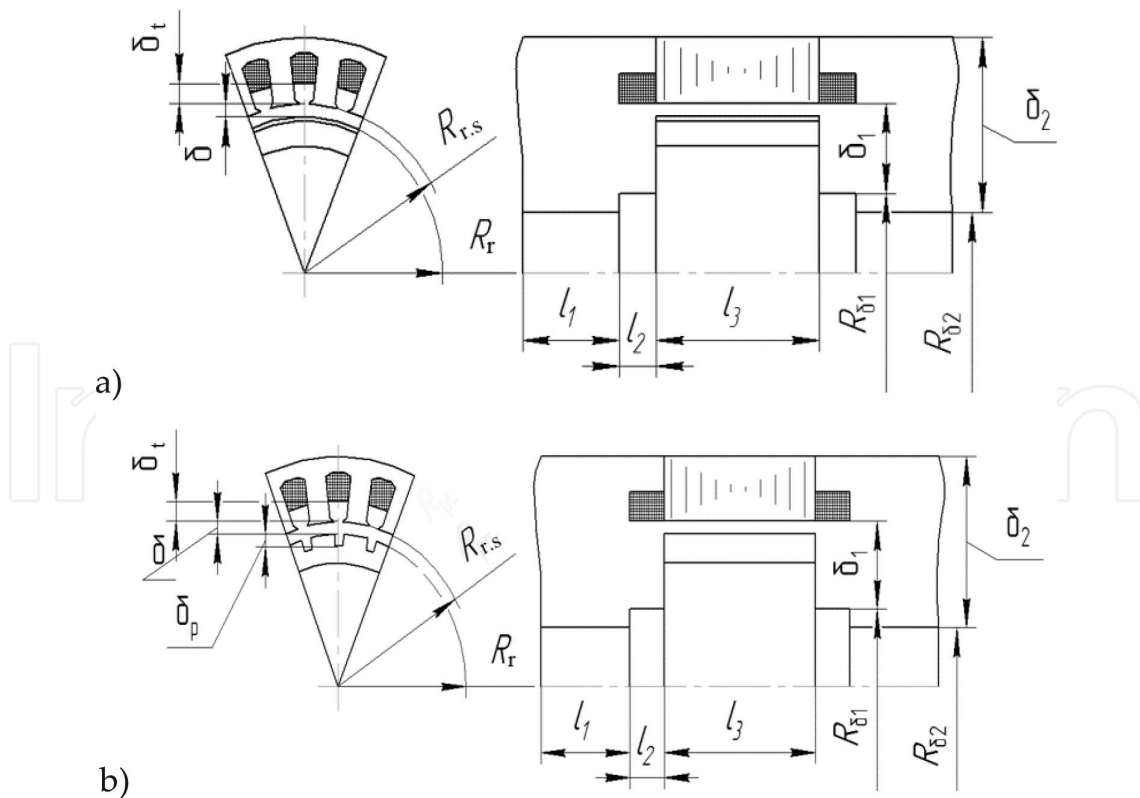


Figure 23. EM designs: (a) smooth rotor and slotted stator and (b) slotted rotor and slotted stator.

The friction coefficient is determined by the Reynolds and Taylor numbers:

$$\text{Re} = \frac{R_r^2 \Omega}{\varsigma}, Ta = \frac{R_r \Omega \delta}{\varsigma} \sqrt{\frac{\delta}{R_r}}, c_f = \frac{1.8}{\text{Re}} \left(\frac{\delta}{R_2} \right)^{-0.25} \frac{R_{s,r}^2}{R_{s,r}^2 - R_r^2}, \quad (23)$$

where ς is a kinematic air viscosity, $R_{s,r}$ is an initial stator radius, δ is an air gap of the EM, and Ω is the rotational speed.

The model with a smooth rotor and a slotted stator is initially considered. The space between the stator and the rotor is represented in the form of two zones: a tooth and a slot, each of which is characterized by a different air gap.

The friction coefficient for slot zone is considered as following:

$$c_{f1} = \frac{1.8}{\text{Re}} \left(\frac{\delta + \delta_t}{R_2} \right)^{-0.25} \frac{R_{s,r}^2}{[R_{s,r} + \delta_t]^2 - R_r^2}, \quad (24)$$

where δ_t is a distance from the tooth to the winding.

For the tooth zone, the friction coefficient is determined from Eq. (9).

Taking into account that the kinematic air viscosity depends on its temperature, the Reynolds number can be rewritten in a general form:

$$\text{Re} = \frac{R_i^2 \Omega}{\varsigma(T, p_a)}, \quad (25)$$

where $\varsigma(T, p_a)$ is a kinematic air viscosity at a certain temperature and pressure, R_i is a rotating part radius of rotor or shaft, and p_a is an air gap pressure.

Taking into account that the air density also depends on the temperature, the windage losses for the slot zone are determined in the following form:

$$P_{\text{slot}} = \frac{1.8}{\text{Re}(R_2)} \left(\frac{\delta + \delta_t}{R_2} \right)^{-0.25} \left[\frac{[R_{s,r} + \delta_t]^2}{[R_{s,r} + \delta_t]^2 - R_r^2} \right] \rho_{\text{air}}(T, p_a) \Omega^3 R_p^3 l_3 \frac{z b_{\Pi}}{2}, \quad (26)$$

and, accordingly, for the tooth zone:

$$P_{\text{tooth}} = \frac{1.8}{\text{Re}(R_2)} \left(\frac{\delta}{R_2} \right)^{-0.25} \left[\frac{R_{s,r}^2}{R_{s,r}^2 - R_r^2} \right] \rho_{\text{air}}(T, p_a) \Omega^3 R_p^3 l_3 \frac{z b_z}{2}, \quad (27)$$

where z is a number of stator teeth, b_z is a tooth width, b_{slot} is a slot width, and $\rho_{\text{air}}(T)$ is an air density at a certain temperature.

Taking into account that the air temperature is the same over the entire surface of the air gap, the total windage losses in the design of **Figure 23a** are defined as:

$$\begin{aligned}
P_{\sum \text{windage}} = & \frac{1.8}{\text{Re}(R_2)} \left(\frac{\delta}{R_r} \right)^{-0.25} \left[\frac{R_{s,r}^2}{R_{s,r}^2 - R_r^2} \right] \rho_{\text{air}}(T, p_a) \Omega^3 R_r^3 l_3 \frac{z b_z}{2} \\
& + \frac{1.8}{\text{Re}(R_2)} \left(\frac{\delta + \delta_t}{R_r} \right)^{-0.25} \left[\frac{[R_{s,r} + \delta_t]^2}{[R_{s,r} + \delta_t]^2 - R_r^2} \right] \rho_{\text{air}}(T, p_a) \Omega^3 R_r^3 l_3 \frac{z b_z}{2} \\
& + \frac{3.6}{\text{Re}(R_{\delta 1})} \left(\frac{\delta_1}{R_{\delta 1}} \right)^{-0.25} \left[\frac{(R_{\delta 1} + \delta_1)^2}{2R_{\delta 1}\delta_1^2 + \delta_1^2} \right] \rho_{\text{air}}(T, p_a) \Omega^3 R_{\delta 1}^4 l_2 \\
& + \frac{3.6}{\text{Re}(R_{\delta 2})} \left(\frac{\delta_2}{R_{\delta 2}} \right)^{-0.25} \left[\frac{(R_{\delta 2} + \delta_2)^2}{2R_{\delta 2}\delta_2^2 + \delta_2^2} \right] \rho_{\text{air}}(T, p_a) \Omega^3 R_{\delta 2}^4 l_1.
\end{aligned} \tag{28}$$

As examples, the energy loss calculations of the EM rotors have been performed at various temperatures in the air gap. The calculations were carried out using two EMs produced by Turbec, which are used in microturbine installations T-100: the 100-kW 60,000-rpm EM with a rotor diameter of 60 mm and the 100-W 500,000 rpm micro-EM with a rotor diameter of 5 mm.

Thus, calculations show that the windage losses largely depend on temperature. With a temperature increase in the air gap from 20 to 60°C, the windage losses increase by 6–7%. The known models of windage losses have a significant error because they do not take into account the stator slots, as well as the temperature influence and pressure in the air gap. Minimal windage losses occur when the inner stator surface is smooth, for example, when slots are filled with a compound.

Minimization of winding losses caused by the stator slots can be achieved by pouring the stator teeth with a compound, or by performing closed stator slots, or by inserting a screen over the entire surface of the air gap. At the same time, the screen will be a technological complication of the EM design. And if it is made of an electrically conductive material, eddy currents will be induced in it and will significantly reduce its efficiency.

For the slotted rotor, the winding loss calculation is similar. However, the slotted rotor surface will cause additional winding losses. Therefore, the rotor and stator surfaces should be smooth; that is, the slots should be filled with a compound or other nonelectrically conductive substances with minimal mass parameters.

Minimal winding losses can be achieved by the operation of high-speed EM with HCPM in vacuum, but it should be taken into account that only certain bearing designs can work stably in a vacuum.

4.7. Efficiency of the high-speed EMs

The efficiency of high-speed EM is determined by the well-known formula:

$$\eta = 100 \left(1 - \frac{\sum P_{\text{loss}}}{P + \sum P_{\text{loss}}} \right), \tag{29}$$

where η is the EM efficiency, $\sum P_{\text{loss}}$ is the total losses, and P is the EM power.

The efficiency of modern EMs reaches high values from 90 to 95%. Even the well-known ultra-high-speed EMs with a rotational speed of up to 800,000 rpm and a power of 50–500 W have an efficiency of 80–90%. The main losses that significantly reduce the efficiency of high-speed EM are the stator magnetic core losses, which increase significantly with increasing magnetization reversal frequency, windage losses, and bearing losses. To reduce these losses and increase the efficiency of ultra-high-speed EMs, various technical solutions are used. For example, AMMs are used to reduce losses in the stator magnetic core. To reduce the friction losses in the rotor, various antifriction coatings or vacuuming of the internal EM cavity are used. To minimize bearing losses, contactless bearings are used.

4.8. Influence of the EM thermal state on the efficiency

As it was shown in the previous sections, the EM temperature has a significant effect on the losses in various EM active elements. Heating of electrical steel leads to a decrease in its specific losses; increasing of the rotor temperature leads to an increase in the friction losses; and heating the winding leads to an increase in resistance. Thus, the EM efficiency is significantly dependent on temperature. Therefore, it seems reasonable to evaluate the dependence of the EM efficiency on temperature. An analysis of the dependence of the EM efficiency on temperature was made by using the example of the high-speed micro-EM produced by Onera [12]. The parameters of this micro-EM are presented in **Table 5**.

It is important to notice that the main consumers of micro-EMs are systems with constant power consumption such as computer systems, navigation systems of unmanned aircrafts. This type of load will lead to the fact that with the decrease of the HCPM energy characteristics, the magnetic flux density in the air gap decreases under the temperature influence. In the calculation result, it was found that for the indicated numerical parameters, the magnetic flux density in the air gap will decrease by 6% at a temperature of 150°C. Under conditions of constant input mechanical power and constant electric power consumption, this will lead to an

Parameters	Value
Power [W]	55
Rotational speed [rpm]	840,000
Outer stator diameter [mm]	25
Active length [mm]	22
Shaft diameter [mm]	4.5
Efficiency [%]	91
Bearing losses [W]	9.7–9.8
Stator magnetic core losses [W]	0.18
Friction losses [W]	2.63
Winding losses [W]	2.33
Total losses [W]	14.84

Table 5. Parameters of the high-speed micro-EM produced by Onera.

Losses	Temperature of the active parts is below 23°C	Temperature of the active parts is 100–110°C after 10 min of operation without a cooling system
Stator magnetic core losses [W]	0.18	0.13
Friction losses [W]	2.63	3.02
Winding losses [W]	2.33	3.88
Efficiency without the bearing losses [%]	91.4	88.6

Table 6. The efficiency comparison of the micro-EM in the cold state and after 10 min of operation without a cooling system.

increase in the linear current load of EM and the current value by also 6%. Taking into account that the copper resistance at a temperature of 100–110°C will also increase by 38%, the winding losses will increase by 55%.

To evaluate the change in the linear current load and the magnetic flux density, an idealized linear dependence of the current and magnetic flux density in the air gap of the micro-EM was adopted. In real EMs, an increase in the linear current load will lead to an increase in the demagnetizing armature reaction action, to additional winding heating, and, consequently, to an increase in the resistance caused by this heating. Preliminary calculations show that in the cold state and 10 min after the start of operation, the winding losses of the real EM can differ by 60–65%. The efficiency comparison of the micro-EM in the cold and heated states (after 10 min of operation without a cooling system) is presented in **Table 6**. With the increase in the EM heat emissions, losses in the active elements increase and, accordingly, the EM efficiency decreases. For the studied numerical values, the efficiency of the micro-EM decreases by 2.8%. This suggests that in the EM design, the efficiency should be calculated at the operating temperature.

5. Conclusion

In this chapter, basics of high-speed EMs with HCPM are presented. The application areas of high-speed EMs are shown. The EM classification is proposed to generalize the theory of high-speed EMs. Practical recommendations for the selection of active and structural components of high-speed EMs are given. The loss determination in high-speed EMs is presented, including methods for determining losses in the stator magnetic cores at high frequencies.

The obtained results can be used in practice in the EM design and in further research.

Author details

Flyur R. Ismagilov, Viacheslav Ye. Vavilov* and Valentina V. Ayguzina

*Address all correspondence to: s2_88@mail.ru

Ufa State Aviation Technical University, Ufa, Russia

References

- [1] Lahne HC, Gerling D. Investigation of high-performance materials in design of a 50000 rpm highspeed induction generator for use in aircraft Applications. In: AST 2015. pp. 1-10
- [2] Lahne HC, Gerling D. Comparison of high-speed highpower machines based on the state of the art. In: 41st Annual Conference of the IEEE Industrial Electronics Society (IECON 2015). 2015. pp. 3519-3524
- [3] Muljadi E, Butterfield CP. Axial flux, modular, permanent-magnet generator with a toroidal winding for wind turbine applications. Industry Applications Conference. 1998;1:174-178
- [4] Caricchi F, Crescimbeni F, Honorati O, Bianco GL. Performance of coreless-winding axial-flux permanent-magnet generator with power output at 400 Hz, 3000 r/min. IEEE Transactions on Industry Applications. 1998;34(6):1263-1269
- [5] Gumerova M, Ismagilov F, Khayrullin I, Vavilov V. Electrodynamical brakes for unmanned aerial vehicles. International Review of Aerospace Engineering (I.R.E.A.S.E). 2014;7(6):202-206
- [6] Szabó L, Oprea C, Viorel I-A, Biró KA. A novel permanent magnet tubular linear generator for wave energy converters. In: Electric Machines & Drives Conference, IEEE International, IEMDC '07; Antalya, Turkey. 2007. pp. 516-521
- [7] Jung S-Y, Choi S-Y, Jung H-K, Choi Y-S, Choi K-M. Performance evaluation of permanent magnet linear generator for charging the battery of mobile apparatus. In: Electric Machines and Drives Conference, IEEE International, IEMDC 2001; Cambridge, MA, USA. 2001. pp. 516-521
- [8] Moore MJ. Micro-turbine Generators. London: Professional Engineering Publishing; 2002. 113 p
- [9] Next-generation microturbines [Internet]. Available from: <https://www.capstoneturbine.com> [Accessed: 2018-03-28]
- [10] Hong DK, Woo BC, Lee JY. Ultra high speed motor supported by air foil bearings for air blower cooling fuel cells. IEEE Transactions on Magnetics. 2012;48:871-874
- [11] Takahashi I, Koganezawa T, Su G. A super high speed PM motor drive system by a quasi-current source inverter. IEEE Transactions on Industrial Electronics. 1994;30(3):683-690
- [12] Guidez J, Ribaud Y, Dessornes O, Courvoisier T. Micro gas turbine research at Onera. In: International Symposium on Measurement and Control in Robotics; Brussels, Belgium. 2005. pp. 1-7
- [13] Borisavljevic A, Polinder H, Ferreira J. On the speed limits of permanent-magnet machines. IEEE Transactions on Industrial Electronics. 2010;57(1):220-227
- [14] Rahman MA, Chiba A, Fukao T. Super high-speed electrical machines—Summary. IEEE Power Engineering Society General Meeting. 2004;2:1272-1275

- [15] Zwyssig C, Kolar JW, Round SD. Mega-speed drive systems: Pushing beyond 1 million RPM. *IEEE/ASME Transactions on Mechatronics*. 2009;**14**(5):564-574
- [16] Zwyssig C, Kolar JW, Round SD. Power electronics interface for a 100 W, 500000 rpm gas turbine portable power unit. In: *Applied Power Electronics Conference*. 2006. pp. 283-289
- [17] Krähenbühl D, Zwyssig C, Weser H, Kolar JW. Mesoscale Electric Power Generation from Pressurized Gas Flow [Internet]. Available from: https://www.pes.ee.ethz.ch/uploads/tx_ethpublications/kraehenbuehl_PowerMEMS07.pdf [Accessed: 2018-03-28]
- [18] Isomura K, Murayama M, Teramoto S, Hikichi K, Endo Y. Experimental verification of the feasibility of a 100W class micro-scale gas turbine at an impeller diameter of 10 mm. *Journal of Micromechanics and Microengineering*. 2006;**16**:254-261
- [19] Park CH, Choi SK, Ham SY. Design and experiment of 400,000 rpm high speed rotor and bearings for 500W class micro gas turbine generator. In: *International Conference on Micro and Nanotechnology for Power Generation and Energy Conversion Applications (PowerMEMS)*. 2011
- [20] Kang S. Fabrication of Functional Mesoscopic Ceramic Parts for Micro Gas Turbine Engines. Sangkyun Kang: Stanford University; 2001. 137 p
- [21] Tüysüz A, Zwyssig C. A novel motor topology for high-speed micro-machining applications. *IEEE Transactions on Industrial Electronics*. 2014;**61**(6):2960-2968
- [22] Borisavljevic A. Limits, Modeling and Design of High-Speed Permanent Magnet Machines. Wormann Print Service; 2011. p. 209
- [23] Westwind [Internet]. Available from: <http://www.westwind-airbearings.com/pcb/index.html> [Accessed: 2018-03-28]
- [24] Sinotech [Internet]. Available from: <http://www.sinotech.com/> [Accessed: 2018-03-28]
- [25] Sirona [Internet]. Available from: <http://www.sirona.com> [Accessed: 2018-03-28]
- [26] Casey MV, Krähenbühl D, Zwyssig C. The design of ultra-high-speed miniature centrifugal compressors. In: *European Conference on Turbomachinery Fluid Dynamics and Thermodynamics ETC 10*. 2013. pp. 1-13
- [27] Kopylov IP. *Electrical Machines (in Russian)*. Moscow: Energoatomizdat; 1986. 360 p
- [28] Goldberg OD. *Design of Electrical Machines (in Russian)*. Moscow: Vysshaya Shkola; 1984. 431 p
- [29] Ledovsky AN. *Electrical Machines with High-coercive Permanent Magnets (in Russian)*. Moscow: Energoatomizdat; 1985. 169 p
- [30] Balagurov VA. *Electric Generators with Permanent Magnets (in Russian)*. Moscow: Energoatomizdat; 1988. 279 p
- [31] Bertinov AI. *Special Electrical Machines. Sources and Converters of Energy (in Russian)*. Moscow: Energoatomizdat; 1982. 552 p

- [32] Co H, Zheng L, Acharya D. Losses in high speed permanent magnet machines used in microturbine applications. *Journal of Engineering for Gas Turbines and Power*. 2009; **131**(2):1-6
- [33] Sharov VS. High-frequency and Superhigh-frequency Electrical Machines (in Russian). Moscow: Energy; 1973. 248 p

IntechOpen

IntechOpen

